# Hydrography of the Labrador Sea during Active Convection

ROBERT S. PICKART AND DANIEL J. TORRES

*Woods Hole Oceanographic Institution, Woods Hole, Massachusetts*

R. ALLYN CLARKE

*Bedford Institute of Oceanography, Dartmouth, Nova Scotia, Canada*

(Manuscript received 6 June 2000, in final form 25 June 2001)

ABSTRACT

The hydrographic structure of the Labrador Sea during wintertime convection is described. The cruise, part of the Deep Convection Experiment, took place in February–March 1997 amidst an extended period of strong forcing in an otherwise moderate winter. Because the water column was preconditioned by previous strong winters, the limited forcing was enough to cause convection to approximately 1500 m. The change in heat storage along a transbasin section, relative to an occupation done the previous October, gives an average heat loss that is consistent with calibrated National Centers for Environmental Prediction surface heat fluxes over that time period ($\sim$200 W m$^{-2}$). Deep overturning was observed both seaward of the western continental slope (which was expected), as well as within the western boundary current itself—something that had not been directly observed previously. These two geographical regions, separated by roughly the 3000-m isobath, produce separate water mass products. The offshore water mass is the familiar cold/fresh/dense classical Labrador Sea Water (LSW). The boundary current water mass is a somewhat warmer, saltier, lighter vintage of classical LSW (though in the far field it would be difficult to distinguish these products). The offshore product was formed within the cyclonic recirculating gyre measured by Lavender et al. in a region that is limited to the north, most likely by an eddy flux of buoyant water from the eastern boundary current. The velocity measurements taken during the cruise provide a transport estimate of the boundary current ''throughput'' and offshore ''recirculation.'' Finally, the overall trends in stratification of the observed mixed layers are described.

## 1. Introduction

The Labrador Sea has long been known as a site of intermediate water formation (Nielsen 1928; Smith et al. 1937; Lazier 1973). Cold air blowing off the Canadian landmass during winter chills the surface waters, which destabilizes the water column and causes deep convection. This overturning—which can extend as deep as two kilometers—forms a water mass known as Labrador Sea Water (LSW), which then spreads into the greater North Atlantic Ocean and beyond. LSW contributes to the global meridional overturning circulation, both directly and via entrainment into the Nordic overflows (e.g., McCartney 1992). It impacts as well the oceanic flux of heat (Talley 2000). The strong signature and convective origin of this water mass helps set the density structure of the subpolar and midlatitude North Atlantic and provides a climate connection between the high-latitude atmosphere and middepth ocean. This connection has been shown to be surprisingly fast at times (e.g., Sy et al. 1997; Pickart et al. 1997b; Molinari et al. 1998).

Despite its importance to the circulation and ventilation of the North Atlantic, much is still unknown about the formation of LSW. This is due in a large part to the harsh environment in which it is formed, rendering in situ observing programs challenging and risky. But our limited knowledge is also due to the intermittency of the convection: in some years LSW is not produced at all (e.g., Lazier 1980). As a result, there have been few observations of newly formed LSW, and these have been limited to measurements isolated in space and time (Clarke and Gascard 1983; Wallace and Lazier 1988). Consequently, there are fundamental questions that are not yet answered regarding the formation and spreading of this important water mass. Among the open questions are: What is the distribution and extent of overturning in the Labrador Basin? What is the relative role of atmospheric forcing versus the ambient stratification/circulation in dictating the convection? And how quickly and by what mechanism(s) does LSW restratify and spread?

It was with such questions in mind that the Labrador Sea Deep Convection Experiment was undertaken. The

*Corresponding author address:* Dr. Robert S. Pickart, Woods Hole Oceanographic Institution, Woods Hole, MA 02543.
E-mail: rpickart@whoi.edu

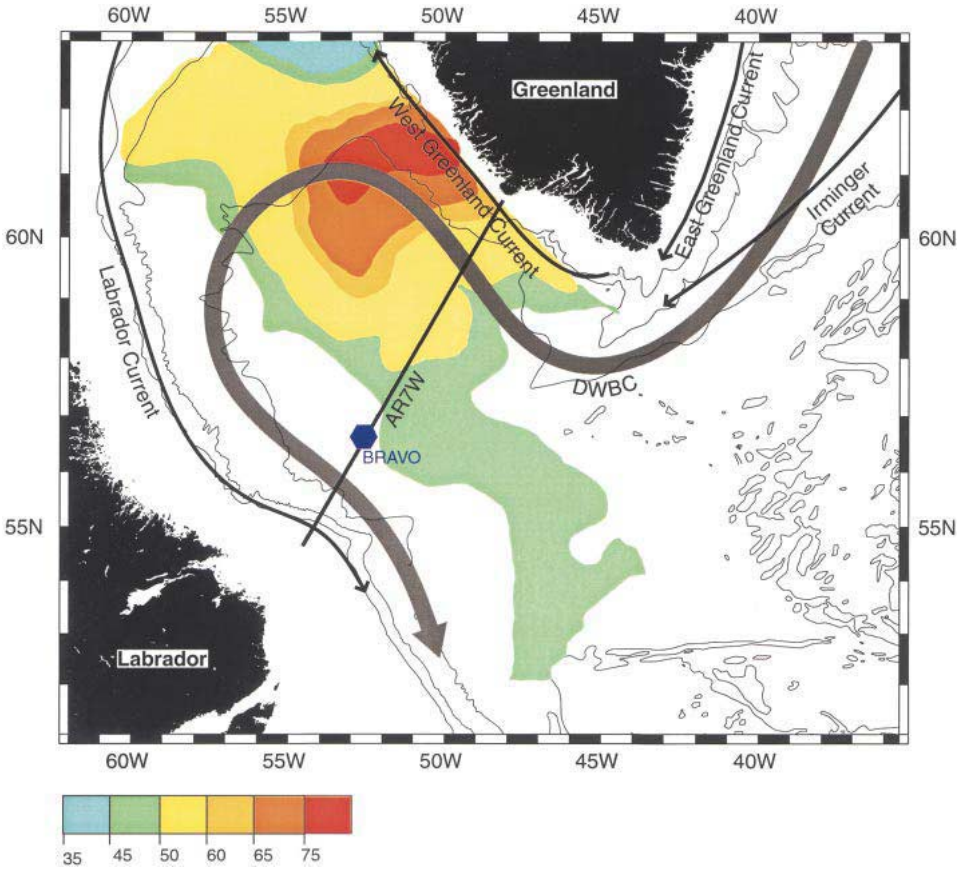


FIG. 1. Boundary currents of the Labrador Sea and the location of the WOCE AR7W hydrographic line and Bravo mooring. The color represents the standard deviation of the sea surface height anomaly (mm) as measured from satellite altimetry (after Prater 2002). The isobaths shown are 1000, 2000, and 3000 m.

overall goal of the program, principally sponsored by the U. S. Office of Naval Research (ONR), was to improve our understanding of the dynamics of high-latitude, open-ocean convection. Details of the Deep Convection Experiment and its different efforts are summarized by the Lab Sea Group (1998). The field phase of the experiment was carried out during the winters of 1996/97 and 1997/98, and consisted of different components addressing the hydrography, circulation, air–sea fluxes, and meteorology associated with convection in the Labrador Sea.

The purpose of this paper is to present the first results from the hydrographic component of the Deep Convection Experiment, which consisted of a seven-week cruise during the winter of 1996/97 (hereafter referred to as the winter of 1997). The cruise covered a large portion of the Labrador Basin, so these measurements represent the first comprehensive description of the Labrador Sea (Fig. 1) during active convection. We present at least partial answers to some of the questions posed above, and also show some unexpected features of the overturning. We begin with a description of the large-scale oceanographic and atmospheric context in which the experiment took place, followed by a more detailed look at the regional hydrographic fields, water mass products, and circulation. Lastly we present a ''macroscopic'' view of the mixed layer properties, revealing some surprising and complex structure.

## 2. Large-scale perspective

A variety of factors conspire to cause deep convection in the Labrador Sea, including the atmospheric forcing, regional circulation (interior and boundary currents), remote input of heat and salt from the Arctic and subtropics, and the Labrador Sea's memory of previous convective seasons. One of the fascinating and complex aspects of LSW formation is its large interannual and decadal variability (e.g., Rhines and Lazier 1995), which likely occurs because so many factors are at work. Perhaps chief among these, or at least a conspicuous indicator of certain key relationships between the different factors, is the North Atlantic Oscillation (NAO). The NAO mode accounts for most of the variance in the large-scale atmospheric patterns of the North Atlantic (Rogers 1990; Hurrell and Dickson 2001). The extent to which this mode is present in a given winter is represented by the NAO index, defined as the normalized

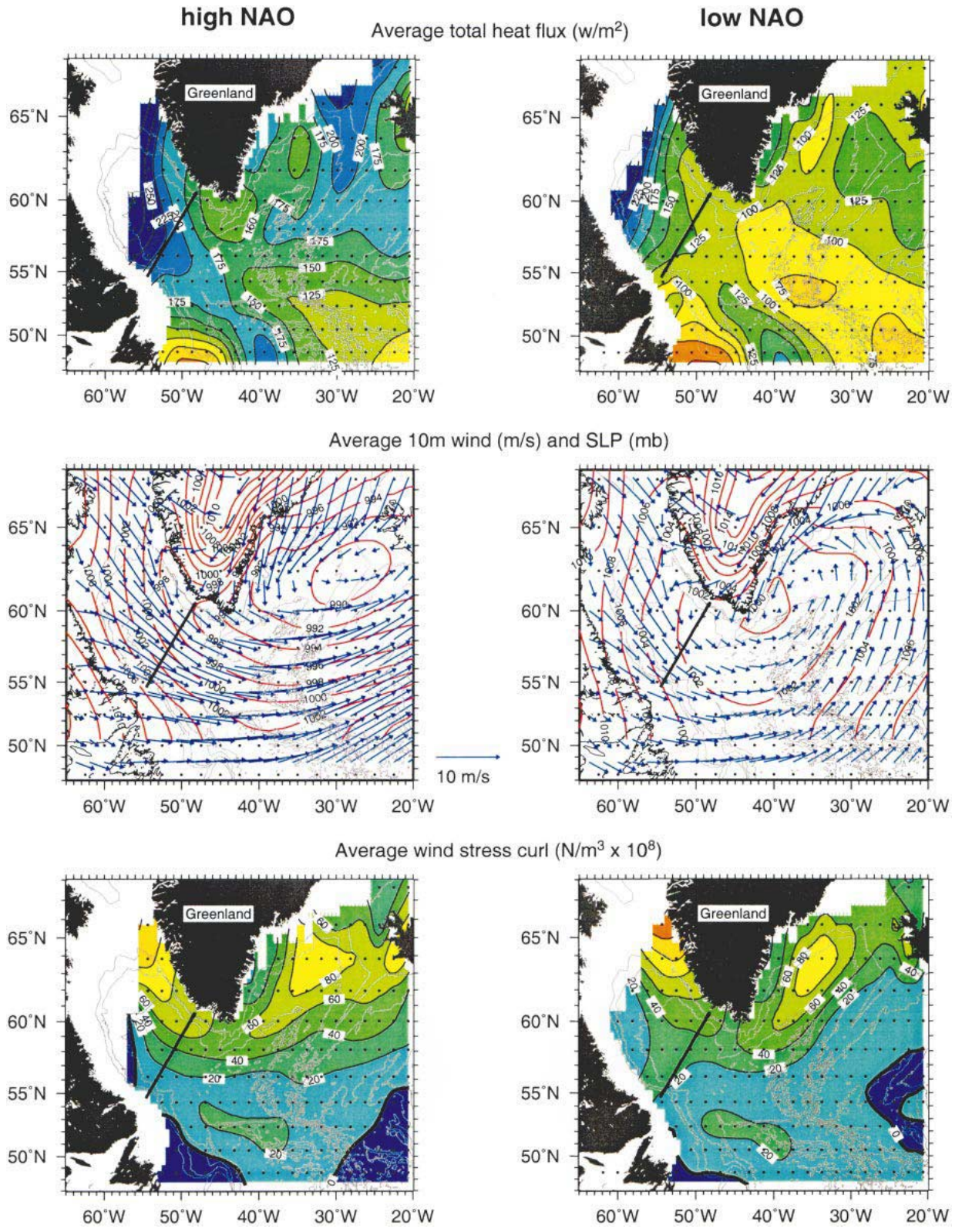


FIG. 2. Averaged calibrated NCEP atmospheric model fields. (left) Average of the three highest NAO winters over the last 20 years (winter is defined as Dec–Mar). (right) Average of the three lowest NAO winters over the last 20 years. The isobaths (gray lines) are 1000, 2000, and 3000 m. The WOCE AR7W hydrographic line is marked.

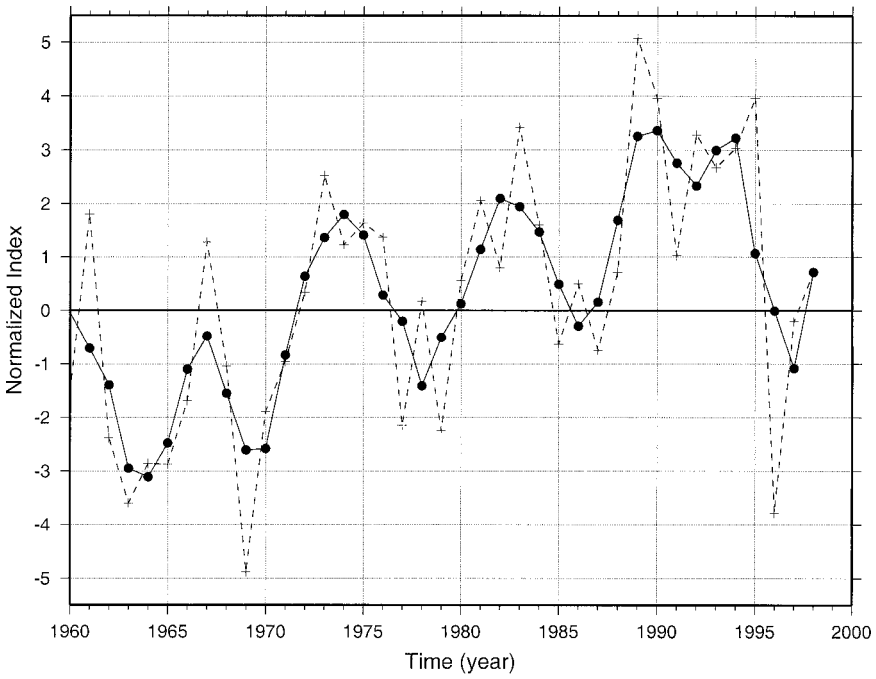


FIG. 3. Time series of the NAO index since 1960: Yearly values (dashed line) and three-point running mean (solid line). See text for the definition of the NAO index.

wintertime sea level pressure difference between Iceland and the Azores (Hurrell 1995). A high NAO index generally means strengthened westerly winds in the subpolar North Atlantic, a more northeasterly orientation of the winter storm track, and a greater number of synoptic low pressure systems that traverse along the track (Rogers 1990; Hurrell and Dickson 2001, manuscript submitted to Oxford University Press).

Dickson et al. (1996) recently demonstrated that the long-term variability of convection in the Labrador Sea varies roughly out of phase with that in the Greenland and Sargasso Seas—and that this coupling is dictated to a large degree by the atmospheric patterns of the NAO. For example, a high NAO state favors convection in the Labrador Sea. During high-NAO winters, the intense lows that pass over the southern Labrador Sea draw cold, dry air from the Labrador continent over the relatively warm surface waters of the sea, causing enhanced air–sea buoyancy fluxes. In situ evidence supports the notion of deepening convection in response to strong values of the NAO (e.g., Curry et al. 1998).

The relationship between the air–sea forcing in the Labrador Sea and the NAO is evident in Fig. 2, which is derived from a 20-yr dataset of reanalyzed National Centers for Environmental Prediction (NCEP) atmospheric model fields (K. Moore 1999, personal communication). These NCEP data have been calibrated (see Renfrew et al. 2002) using in situ measurements collected during the Deep Convection hydrographic cruise and, hence, constitute the most realistic depiction of the atmospheric forcing obtained to date for this remote region. Their reasonable degree of accuracy is supported by the heat storage calculation presented in section 4. Note in Fig. 2 that the region of highest heat loss—located in the northwestern Labrador Sea—extends considerably more southward in high NAO years, in concert with enhanced westerly winds in the southern part of the basin. In low NAO years the winds tend to be weaker and more northerly, both of which result in less cold air over the Labrador Sea. Regardless of the NAO, the wind stress curl is significantly enhanced on either side of Greenland.

It is tempting to emphasize the notion of a ''linear'' NAO-driven convective system in the Labrador Sea (i.e., high NAO means intense convection, low NAO means little or no convection). For example, the extended period of high NAO in the late 1980s/early 1990s (Fig. 3) was accompanied by deep convection to 2300 m in the Labrador Sea (Lazier et al. 2001), and during this time large amounts of LSW were detected both in the eastern North Atlantic (e.g., Sy et al. 1997) and to the south in the deep western boundary current (e.g., Pickart et al. 1997b). However, as highlighted in Dickson et al. (1996), such a notion is an oversimplification in light of all the different factors influencing convection. For instance, the ''Great Salinity Anomaly'' in the early 1970s (Dickson et al. 1988) covered the surface of the Labrador Sea with a layer of freshwater, undoubtedly modulating the convection during that time period (Talley and McCartney 1982). Dickson et al. (1996) characterize the impact of the Great Salinity

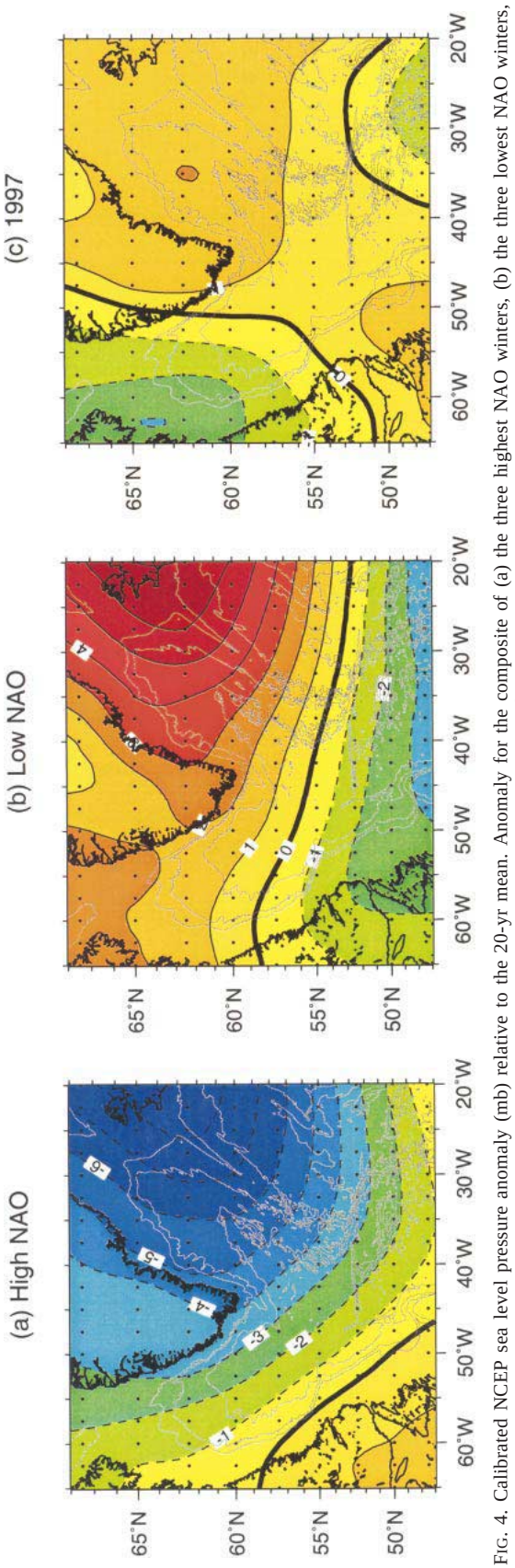


FIG. 4. Calibrated NCEP sea level pressure anomaly (mb) relative to the 20-yr mean. Anomaly for the composite of (a) the three highest NAO winters, (b) the three lowest NAO winters, (c) the individual winter of 1997.

Anomaly as a remote (delayed) response to the strengthening of the East Greenland Current—which in turn resulted from increased northerly winds east of Greenland during low NAO conditions (Dickson et al. 1988). This represents an extreme example of Arctic freshwater export influencing convection via the shelfbreak portion of the rim-current system in the Labrador Sea (i.e., the East Greenland–West Greenland–Labrador Currents; Fig. 1). Belkin et al. (1998) suggest that such freshwater pulses are not uncommon. Offshore of the shelf break, the slopewater part of the rim current transports warm and salty Irminger water (North Atlantic Current remnant water: Fig. 1), which also likely impacts LSW formation.[1] The input of this water from the subtropics is known to vary interannually [although the baroclinic component of this input is believed to have an NAO connection as well (Curry and McCartney 2001)].

As mentioned above, the Labrador Sea also has a memory of previous winters, due to the fact that not all of the newly formed LSW flushes out of the basin in a year's time. This memory, together with the interior circulation, impacts the ability for convection to occur. For example, during periods of weak convection a buoyant density cap can begin to develop over the sea, making it increasingly difficult for the atmospheric forcing to ''punch through'' in succeeding years. This situation occurred in the 1960s (Lazier 1980). The opposite extreme is when repeated winters of strong convection produce a large body of weakly stratified water in the center of the basin, which is conducive for future overturning, even with moderate forcing. By parameterizing the ocean's ability to integrate the effect of external forcing over time, the simple model of Straneo and Pickart (2001) produces a more accurate representation of the Labrador Sea convective record than an NAO-only scenario.

What were the conditions under which the Deep Convection Experiment took place? Consider first the NAO index. As seen in Fig. 3, the index dropped sharply in 1996 after an extended period of high values, and remained negative the following winter (i.e., the year of the hydrographic cruise). Taken at face value, two successive negative NAO winters might imply a weak convection year in the Labrador Sea. However, we observed mixed layers as deep as 1500 m. Upon closer inspection, 1997 did not fall into either the canonical high or low NAO regime. This can be seen in the sea level pressure anomaly maps constructed from the calibrated NCEP fields (Fig. 4, where the anomaly is relative to the 20-yr mean). Not only is the 1997 anomaly weak (i.e., neither high nor low), but the spatial pattern is a dipole-like structure, oppositely signed in the Labrador and Irminger Seas.

[1] In this paper we refer to Irminger Water as the anomalously warm and salty water being transported by the boundary current, as opposed to the winter mixed water formed in the interior of the Irminger Basin, which historically has also been called Irminger Water.

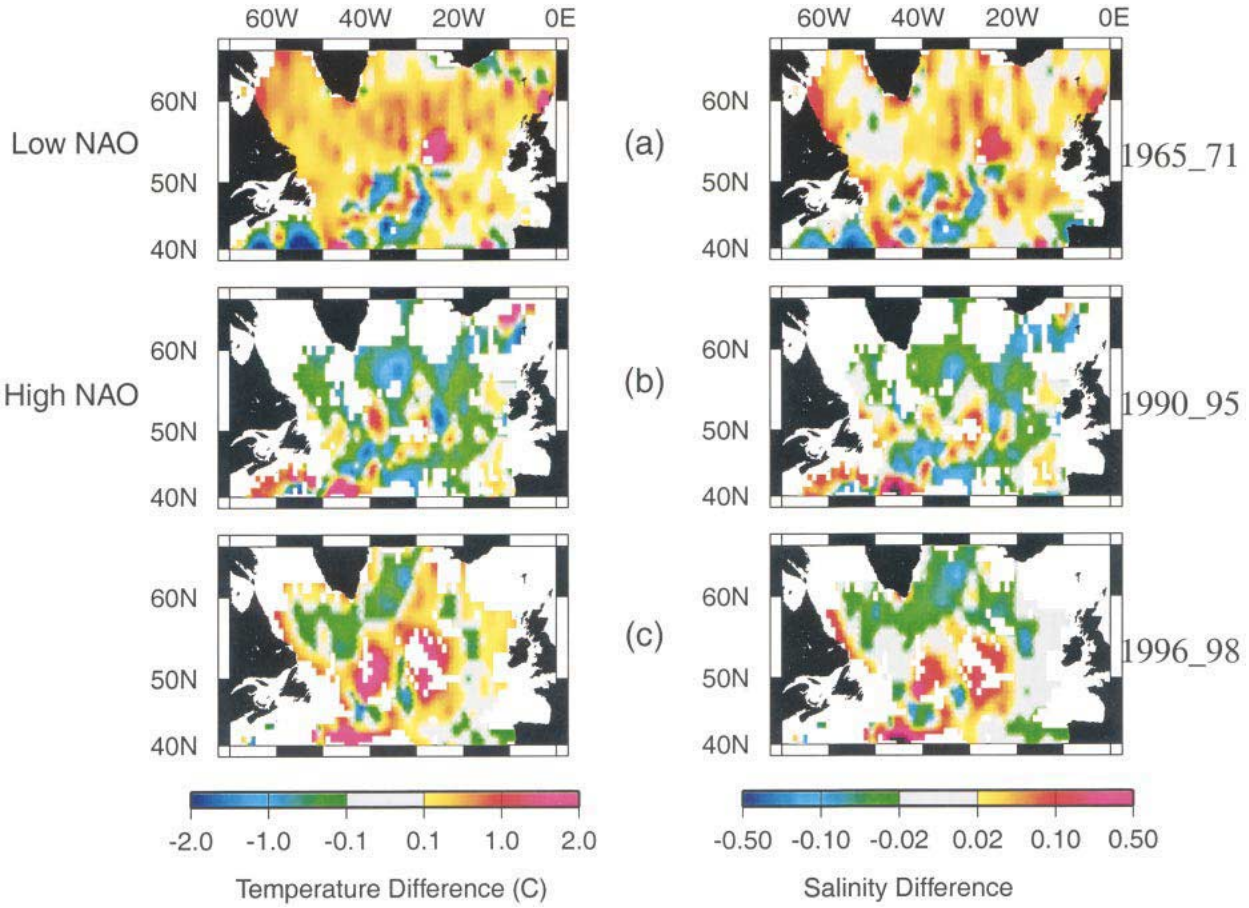


FIG. 5. Anomaly of temperature (left) and salinity (right) at 400 m in the subpolar North Atlantic for three time periods, compared to the long-term climatological average (after Curry and McCartney 2001). (a) 1965–71 (a low NAO period), (b) 1990–95 (a high NAO period), and (c) the time period of the Deep Convection Experiment.

Regarding the state of the ocean, Curry and McCartney (2001) recently constructed large-scale maps of temperature and salinity for the subpolar gyre for different time periods. Figure 5 shows that during the time period of the experiment, 1996–98, the subpolar gyre did not fall into either the low- or high-NAO regime as well. In the low-NAO state (Fig. 5a), the entire upper layer of the subpolar gyre is warm and salty (compared to climatology), while in the high-NAO state it is markedly colder and fresher (Fig. 5b). Our experiment took place during a complex ''transition phase,'' where enhanced export of warm and salty subtropical water had already flooded the boundary current system of the subpolar gyre, while the interior portions of the gyre (including the Labrador Sea) were still colder and fresher than average.

It is enlightening to diagnose further the particular winter of 1997 using the NCEP climatology. Figure 6 shows the total heat flux averaged over the Labrador Basin, broken down by both winter and month of winter. While the winter-averaged heat loss (solid curve in Fig. 6) is significantly correlated at the 99% confidence level with the yearly NAO index, there is large scatter in the monthly heat loss values (discrete symbols in Fig. 6). Interestingly, the three years during which December experienced the largest monthly heat flux were low NAO years, whereas in five out of the seven highest-NAO years January was the month of strongest heat loss. Note the skewness in 1997, showing that February (i.e., during the hydrographic cruise) was anomalously cold that year. In fact, even though 1997 had the fourth lowest NAO during the 20-yr time period, February 1997 had the second largest heat loss of all Februaries. This was largely due to strong winds and, hence, an especially strong latent heat loss. The two other high skewness years (discounting 1995, which had a very small standard deviation) were 1993 and 1982. The former was an extremely strong winter, resulting in the deepest convection on record (J. Lazier 1999, personal communication). The latter was much like 1997, an overall moderate winter with a particularly strong February. However, four out of the five years preceding 1982 were moderate to low-NAO years, whereas four of the five years prior to 1997 had extremely high NAO

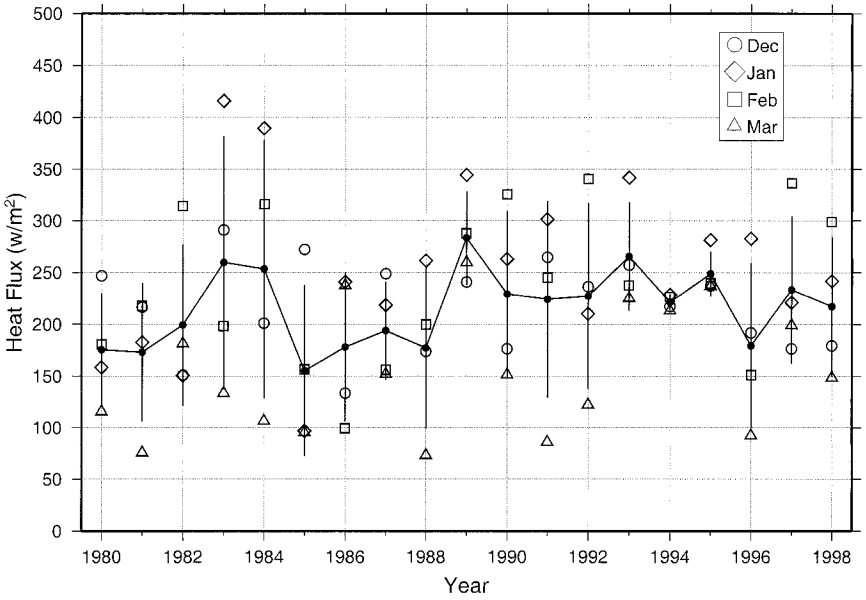


FIG. 6. Calibrated NCEP total heat flux averaged over the Labrador Sea. Winter mean values and standard deviations are shown (solid circles and lines), along with the monthly averages for a given winter (open symbols).

values. Hence the system was primed in 1997 so that a single month of intense forcing was enough to cause deep overturning. Presumably this was not the case in 1982, although this cannot be verified because no data were collected that year.

In summary, 1997 was an overall moderate winter—one that was neither a canonical high- nor low- NAO year in terms of the atmospheric conditions or state of the subpolar gyre. However, the hydrographic cruise took place during a ''microcosm'' of classic Labrador Sea convective forcing in the harsh month of February 1997, when the ocean was well preconditioned from previous years.

## 3. Hydrographic cruise

A hydrographic cruise was carried out on the Research Vessel *Knorr,* which departed Halifax, Nova Scotia, on 2 February 1997 and returned to Woods Hole, Massachusetts, on 20 March 1997 (Fig. 7). As indicated by the NCEP climatology, we experienced conditions conducive for overturning: frequent storms, cold air temperatures, and strong winds. The mean air temperature was $-8$°C (rising above 0°C on only one day). The mean wind speed was 12 m $s^{-1}$ (gusting to more than 25 m $s^{-1}$), blowing on average out of the west-northwest. Storms arrived, and the sea state built, in a surprisingly short amount of time. It snowed constantly, and white-out conditions frequently reduced visibility to near-zero. Operationally, one of our biggest challenges was keeping the decks and bulwarks free of ice. The cold air, together with the large amount of sea spray and wash, caused ice to build up quickly. Consequently, the crew (with occasional help from the science party) would regularly knock ice off the vessel using wooden mallets and snow shovels.

Ice in the water was also a problem during the cruise, since the *Knorr* is not ice-strengthened. While the center of the Labrador Sea is free of ice, the boundaries are not. On the Greenland side the problem was icebergs (advected into the area by the East/West Greenland Current), in particular the smaller bergs not easily detected on ship's radar. During our second visit to the Greenland coast numerous icebergs cluttered the working area, including one that caused us to divert our station track. On the Labrador side the problem was pack ice. Here we experienced the coldest weather of the cruise ($-17$°C) and were clearly at a disadvantage by not having an ice-strengthened hull. The reason for sampling near the western shelf break is that the highest buoyancy fluxes occur just seaward of the ice edge, and we suspected that convection might be occurring here as well as in the central part of the basin.

Figure 7 shows the locations of the hydrographic stations occupied. Each of the conductivity–temperature–depth (CTD) casts extended to the bottom and included measurement of dissolved oxygen, at typically 24 levels. Other tracers were measured at a subset of the stations, including chlorofluorocarbons and tritium–helium (Lamont-Doherty Geological Observatory). A lowered acoustic Doppler current profiler (LADCP) was attached to the instrument package, providing a vertical profile of absolute horizontal velocity. Three different CTDs were used during the course of the cruise, two EG&G

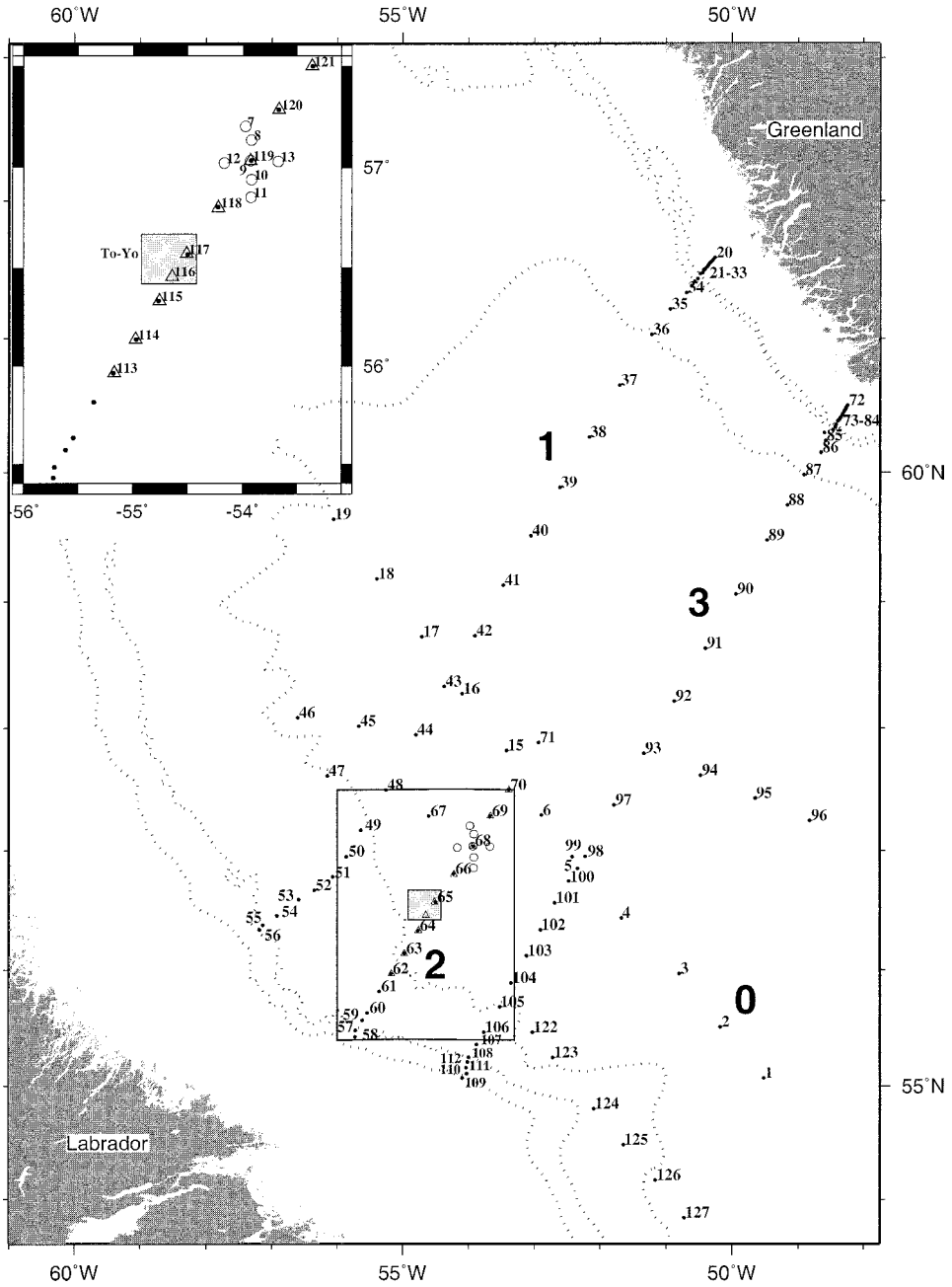


FIG. 7. Hydrographic stations occupied during Feb–Mar 1997 (section numbers are marked in bold). A portion of Section 2 was occupied twice (separated by 10 days): stations 57–71 comprise the first occupation (solid circles), and stations 113–121 the second occupation (open triangles, see insert). Stations 7–13 (open circles, insert) coincided with a small-scale intensive float deployment early in the cruise. The location of the second to-yo CTD survey is indicated by the shaded box. The isobaths shown are 1000, 2000, and 3000 m.

Mark-III instruments, and a Falmouth Scientific Instruments integrated CTD. Details of instrument performance and calibration are found in Zimmermann et al. (2000). The temperature accuracy was determined via pre- and postcruise laboratory calibrations, and the salinity accuracy calculated by comparison with the in situ bottle data. Salinity is reported using the practical salinity scale. The overall accuracy of the measurements was 0.001°C for temperature, and 0.0025 for salinity. An exception to this is the group of stations on the Greenland shelf, which not surprisingly exhibited a higher salinity standard deviation (0.01) compared to the bottle data. No shelf data are considered in this paper. It is worth noting that oftentimes the upcast trace of the

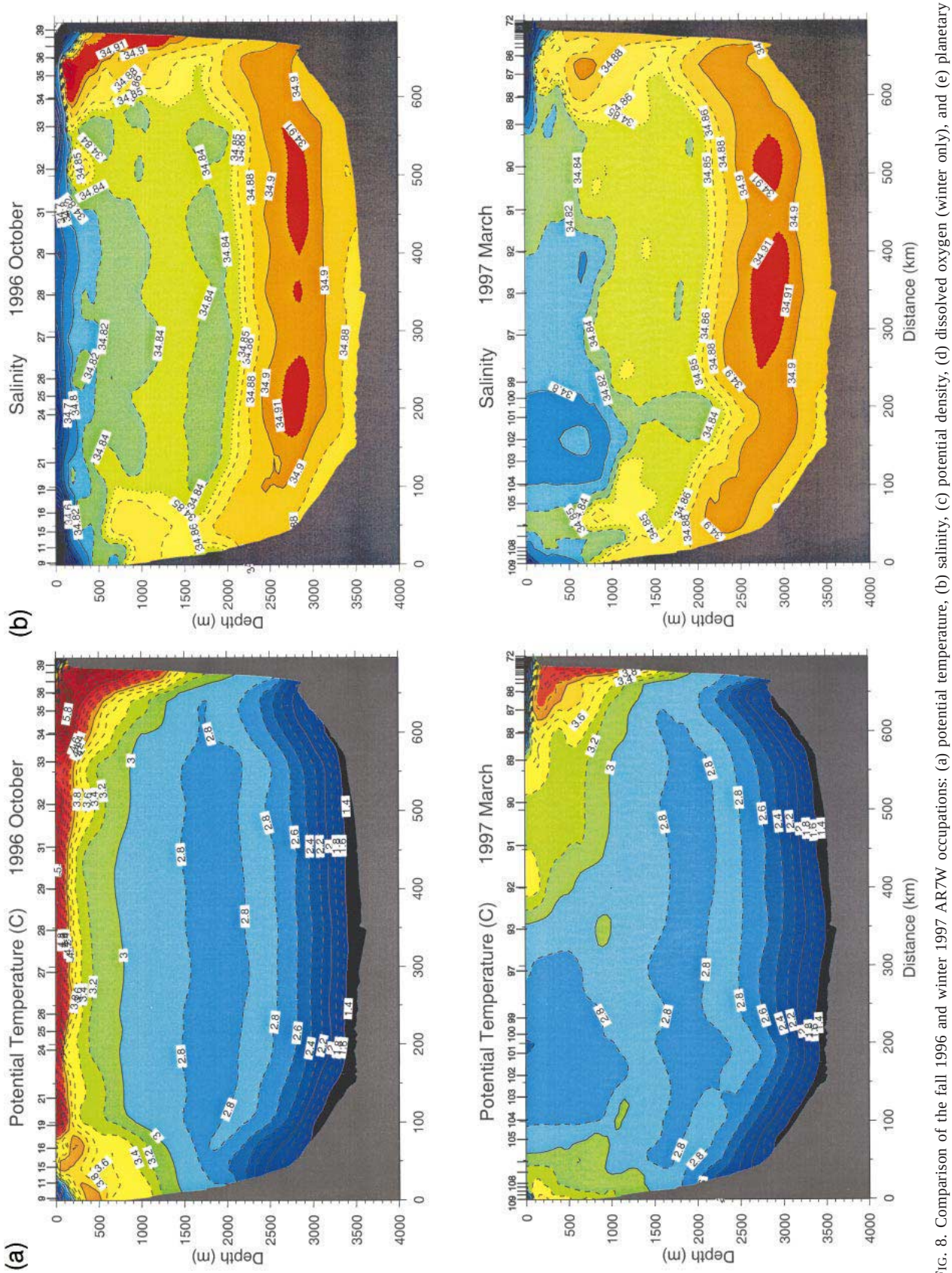


FIG. 8. Comparison of the fall 1996 and winter 1997 AR7W occupations: (a) potential temperature, (b) salinity, (c) potential density, (d) dissolved oxygen (winter only), and (e) planetary potential vorticity.

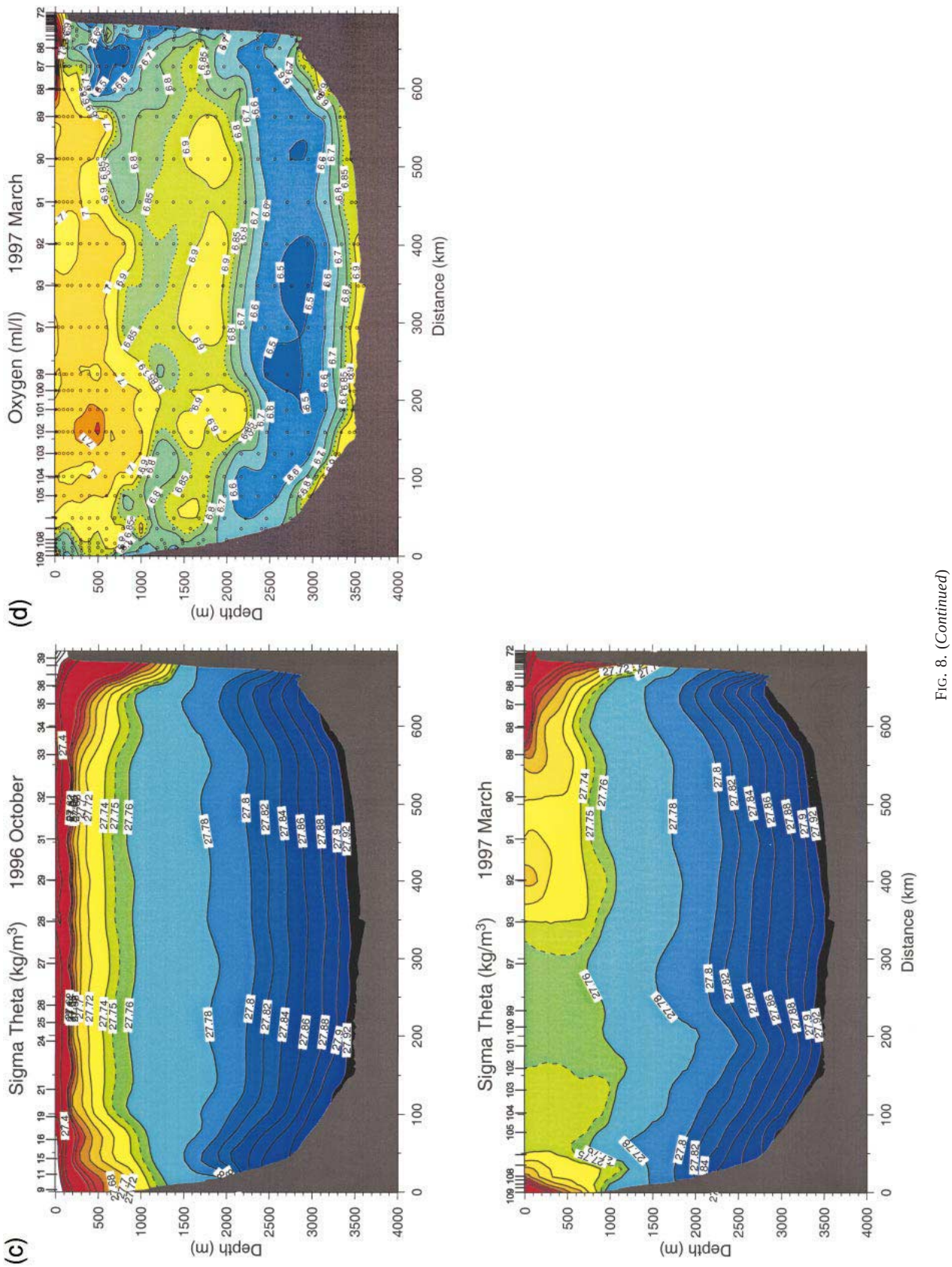


FIG. 8. (*Continued*)

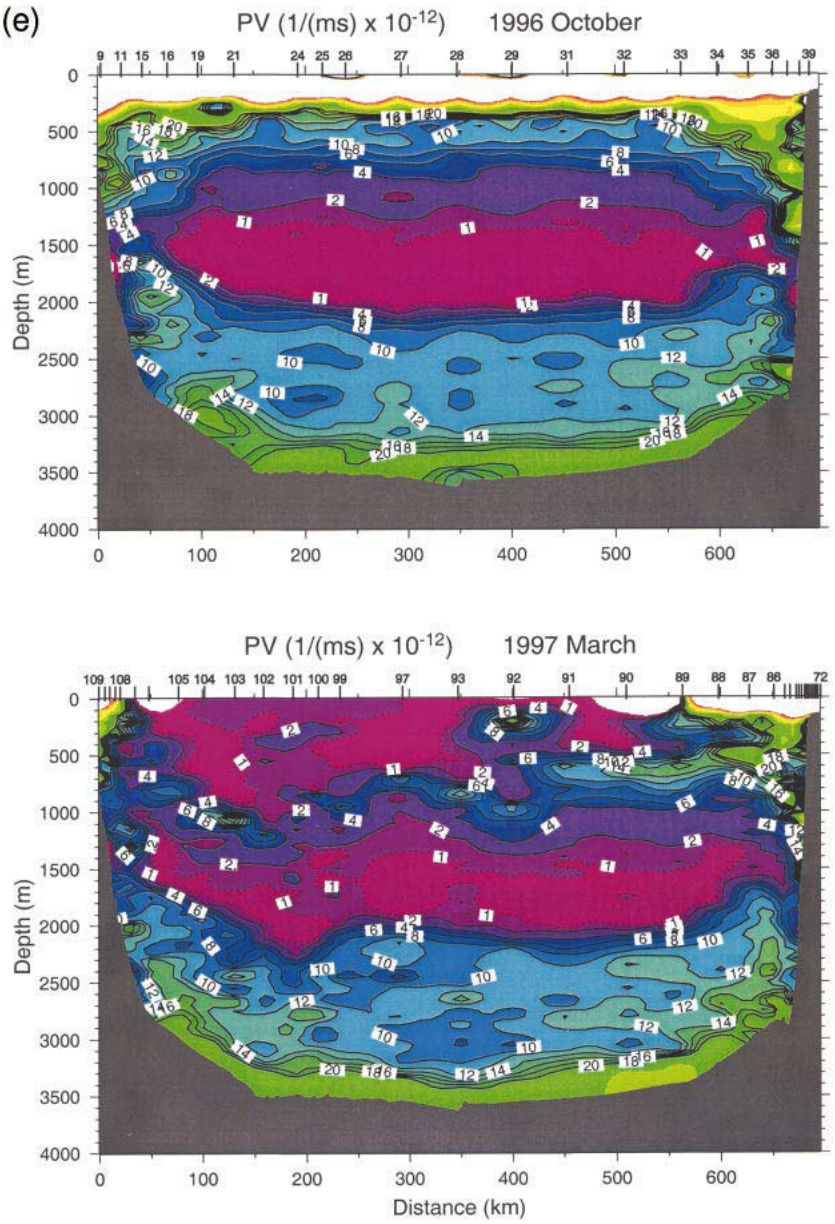


FIG. 8. *(Continued)*

CTD differed significantly from the downcast trace, a testament to the pronounced small-scale variability present during convection. Such variability has also been observed in the convective regions of the Mediterranean Sea (Schott et al. 1996) and the Greenland Sea (Schott et al. 1993).

We adopted a multifaceted approach to our survey pattern. We wanted to describe the basinwide state of the sea, including the rim current system; at the same time we sought increased resolution in the western part of the basin where the strongest air–sea forcing occurs (and previous work suggested the deepest mixed layers would be found). Both the alongbasin line (Section 0) and the southern cross-basin line (Section 3) were repeats of the fall 1996 hydrographic cruise done by the Bedford Institute of Oceanography as part of the Deep Convection Experiment. The southern line was the first wintertime occupation of the World Ocean Circulation Experiment (WOCE) AR7W section. Note that the three western boundary crossings did not extend onto the shelf: this was due to the proximity of the ice edge. Finally, we wanted to do small-scale mapping of a convective feature if the opportunity arose. Toward this end we conducted two ''to-yo'' CTD surveys, including a 36-h survey at the end of the cruise that sampled the deepest mixed layers of the experiment (Fig. 7). These

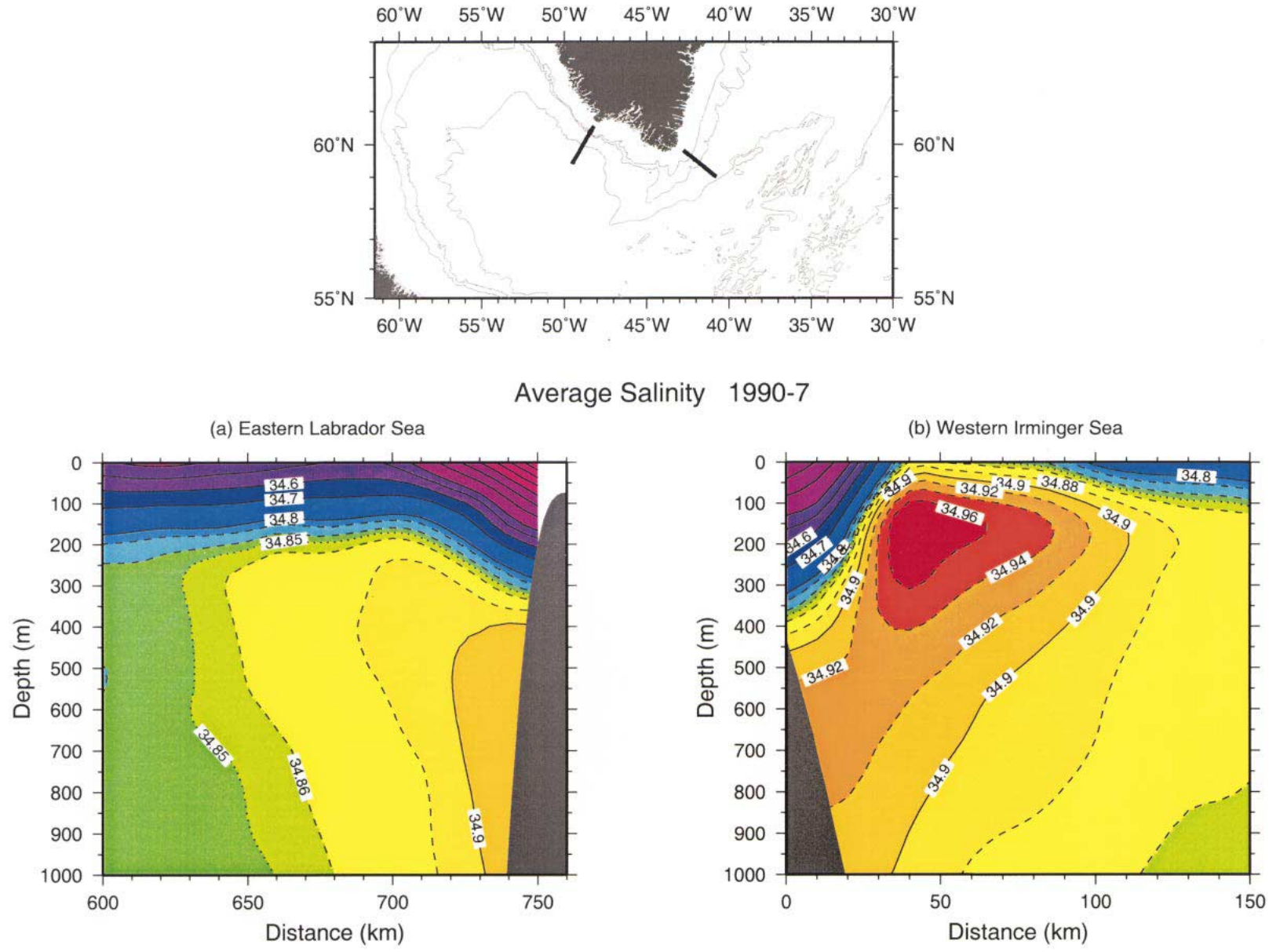


FIG. 9. Mean upper-layer salinity sections for the period 1990–97 (see P01a). (top) The locations of the two mean sections. The isobaths are 1000, 2000, and 3000 m: (bottom) (a) Eastern Labrador Sea; (b) western Irminger Sea.

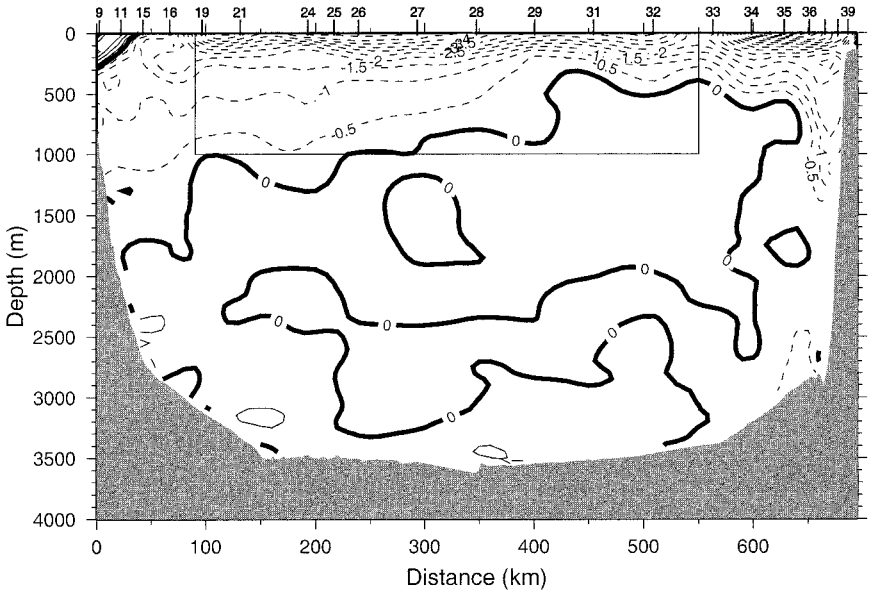


FIG. 10. Change in heat storage (PJ km$^{-1}$) along AR7W from fall 1996 to winter 1997.

high-resolution data will be the subject of a separate paper. The middle cross-basin line (Section 2), located in the region of the most intense convective activity, was occupied a second time late in the cruise (inset of Fig. 7).

The hydrographic cruise also served as a platform for some of the other observational components of the Deep Convection Experiment (see other articles in this special issue). This included studies of the atmospheric conditions, air–sea fluxes, and Lagrangian circulation. In all, seven types of Lagrangian instruments were deployed during the cruise. This included a high-density deployment of ''Fully Lagrangian Drifters'' (Steffen and D'Asaro 2002) at the start of the cruise, which is the reason for the cluster of CTD stations near the northern end of Section 2. All subsurface floats (and the majority of the surface drifters) were deployed at CTD stations. For more details regarding the activities and operations on the cruise, the reader is referred to Pickart (1997), Pickart et al. (1997a), and the Lab Sea Group (1998).

## 4. Vertical view of convection

### *a. Temperature and salinity*

For more than a decade the Bedford Institute of Oceanography has been occupying the WOCE AR7W CTD section across the Labrador Sea (Fig. 1). The cruise typically takes place in spring, after the convective season. The Deep Convection Experiment provided the first opportunity to occupy this line during the period of active overturning. It is instructive to consider this section in detail, which we do here in relation to the 1996 fall occupation (done 4 months prior to the winter cruise). The comparison is shown in Fig. 8. It should be noted that this section is a bit south of the region of deepest convection, at least in the winter of 1997.

In the fall section note the buoyant upper layer present over the entire basin, and the rim-current properties on both sides of the section. The warm, salty Irminger Water (centered near 500 m on the Greenland side; Figs. 8a,b) is significantly eroded by the time it reaches the Labrador side. This is presumably due to isopycnal mixing along the path of the rim current as it encircles the basin (Cuny et al. 2002), since very little of this water mass continues northward through Davis Strait (Ross 1992).

In the winter section the stratified upper layer has been eroded away, and a region of cold, fresh newly formed LSW is seen in the western part of the basin, extending to depths greater than 1000 m (Figs. 8a,b). This is the area where previous studies have observed newly ventilated LSW. Note that the rim current potential temperature ($\theta$) and salinity ($S$) distributions are also quite different in the winter. On the Labrador side this is easily explained: the Irminger Water has been vertically mixed due to convection within the boundary current, producing a warmer and saltier vintage of LSW (see next section). This phenomenon was not observed in any of the past experiments, possibly because the boundary current region restratifies so quickly. On the Greenland side, the wintertime cooling and freshening of the Irminger Water is more of a puzzle. Note the pronounced cold, fresh cap over the rim current here. This (presumably with the weaker air–sea flux on the eastern side of the basin) prevented convection from occurring here during the experiment. So what caused the change in the Irminger properties off of West Greenland? One possibility is that it was due to a change in

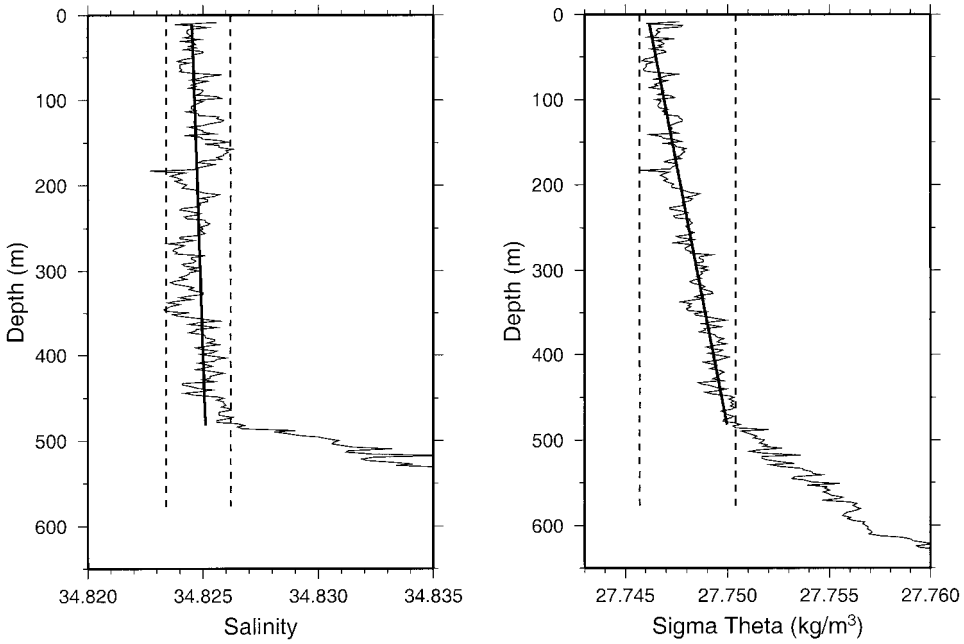


FIG. 11. Example of the criterion for determining mixed layer depth (see text for details) using station 115 profiles. The linear fit is shown as well.

the subtropical source input, but as noted earlier the overall rim-current system of the subpolar gyre was becoming warmer and saltier during this time frame.

Another more plausible explanation is that ventilation occurred within the boundary current upstream of this location, in particular on the eastern side of Greenland. This is consistent with the results of Pickart et al. 2001; manuscript submitted to *Deep-Sea Res.* (hereafter P01a), who present evidence that deep overturning also occurs in the Irminger Basin. Using the mean sections constructed by P01a (Fig. 9), one sees that the cold, fresh Arctic waters of the shelfbreak current are more effectively trapped to the boundary east of Greenland than west of Greenland. This means that a buoyant cap does not typically extend over the continental slope in the Irminger Basin, in contrast to the Labrador Basin (as seen in Fig. 9). This, together with the enhanced air–sea forcing east of the Greenland landmass (see P01a) makes it more favorable for convection to occur over the eastern slope of Greenland than over the western slope of Greenland. Thus, we pose the following scenario [consistent with the view put forth by Smith et al. (1937)]: The Irminger Water in the rim current is partially ventilated east of Greenland in the Irminger Basin; it then rounds Cape Farewell and ''subducts'' under the cold, fresh cap extending off of the West Greenland boundary. As noted above, a second area where (more robust) Irminger Water ventilation occurs is next to the Labrador boundary, where the air–sea forcing is particularly strong.

The question now is, why does the buoyant shelfbreak water extend offshore on the west side of Greenland but not the east side of Greenland? One reason might be due to the enhanced eddy activity on the western side, as seen in Fig. 1. There is now strong evidence that the rim current system in the eastern Labrador Sea is particularly unstable and, hence, is a source of eddies (Prater 2002; Lavender 2001; Lilly et al. 2001a,b, manuscripts submitted to *J. Phys. Oceanogr.*, hereafter L01a and L01b, respectively; Cuny 2002). The eddy variability is maximum in the region where the continental slope broadens abruptly near 61.5°N (where the 3000-m isobath ''turns the corner;'' Fig. 1). We conjecture that the eddy generation in this area results in an enhanced offshore flux of shelfbreak water, contributing to the freshwater cap in the eastern Labrador Sea (a process that is seemingly absent in the Irminger Sea). This view is supported by the results of L01a, who have observed surface-intensified ''Irminger rings'' in the central Labrador Sea, which, via their altimetric signal, are believed to emanate from the region of elevated eddy energy (L01b). Note that the AR7W section is near the southern edge of the region of enhanced eddy variability (Fig. 1).

Clearly these ideas require further investigation, but we feel compelled to present such a scenario as an attempt to explain the seasonal change in $\theta$ and $S$ observed in the rim current. Other aspects of the winter dataset, presented below, support this eddy flux interpretation as well.

### *b. Density*

The sections of potential density referenced to the sea surface ($\sigma_\theta$, Fig. 8c) show many of the features de-

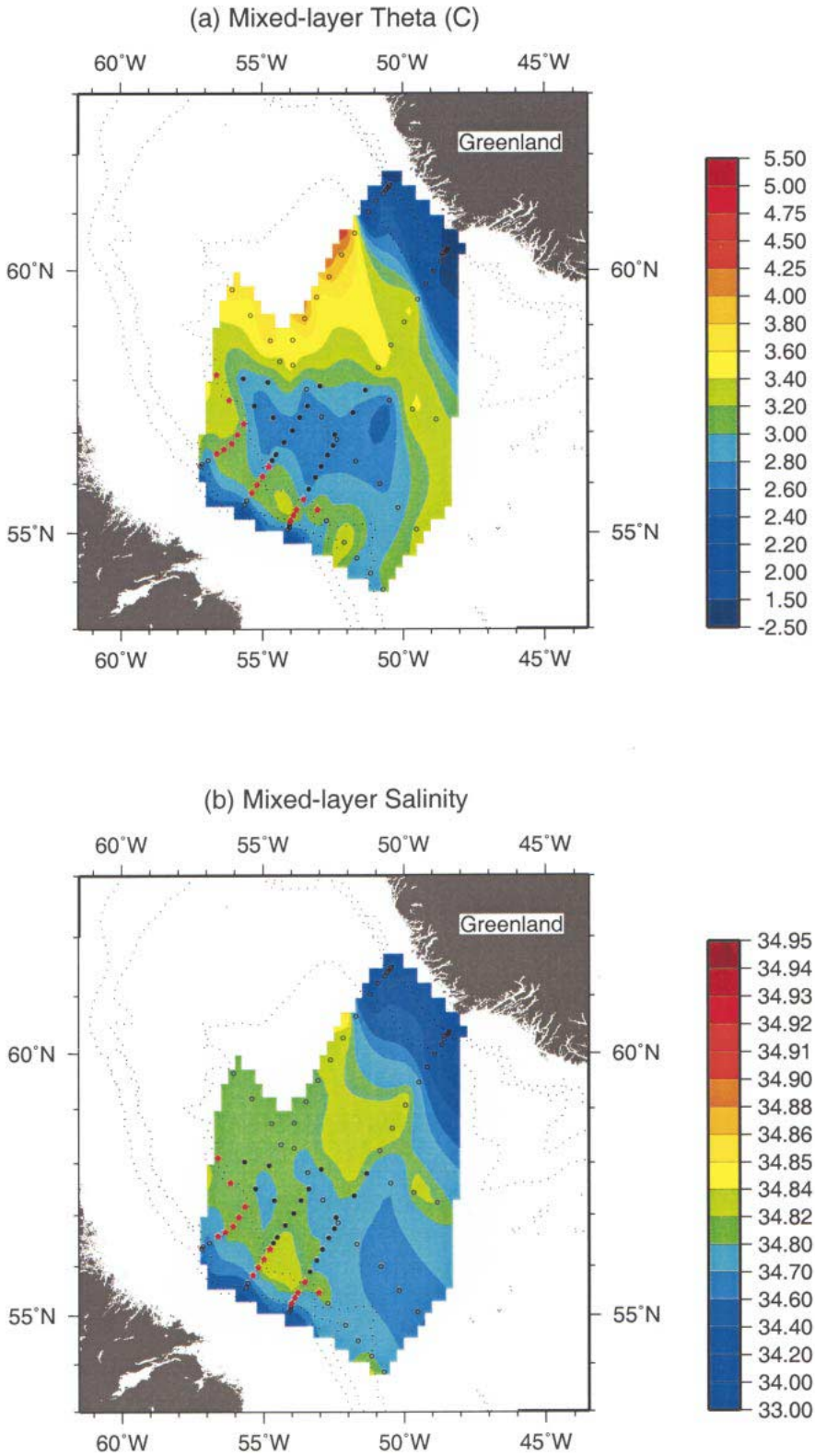


FIG. 12. Lateral distributions of mixed layer properties. Station positions are marked by the discrete symbols, where solid red stars denote the boundary product stations and solid black circles indicate gyre product stations (Section 0 is excluded from this classification). The isobaths shown are 1000, 2000, and 3000 m. (a) Potential temperature, (b) salinity, (c) potential density, (d) depth (e) $\theta$–$S$ of boundary product stations (solid red stars) and gyre product stations (solid black circles).

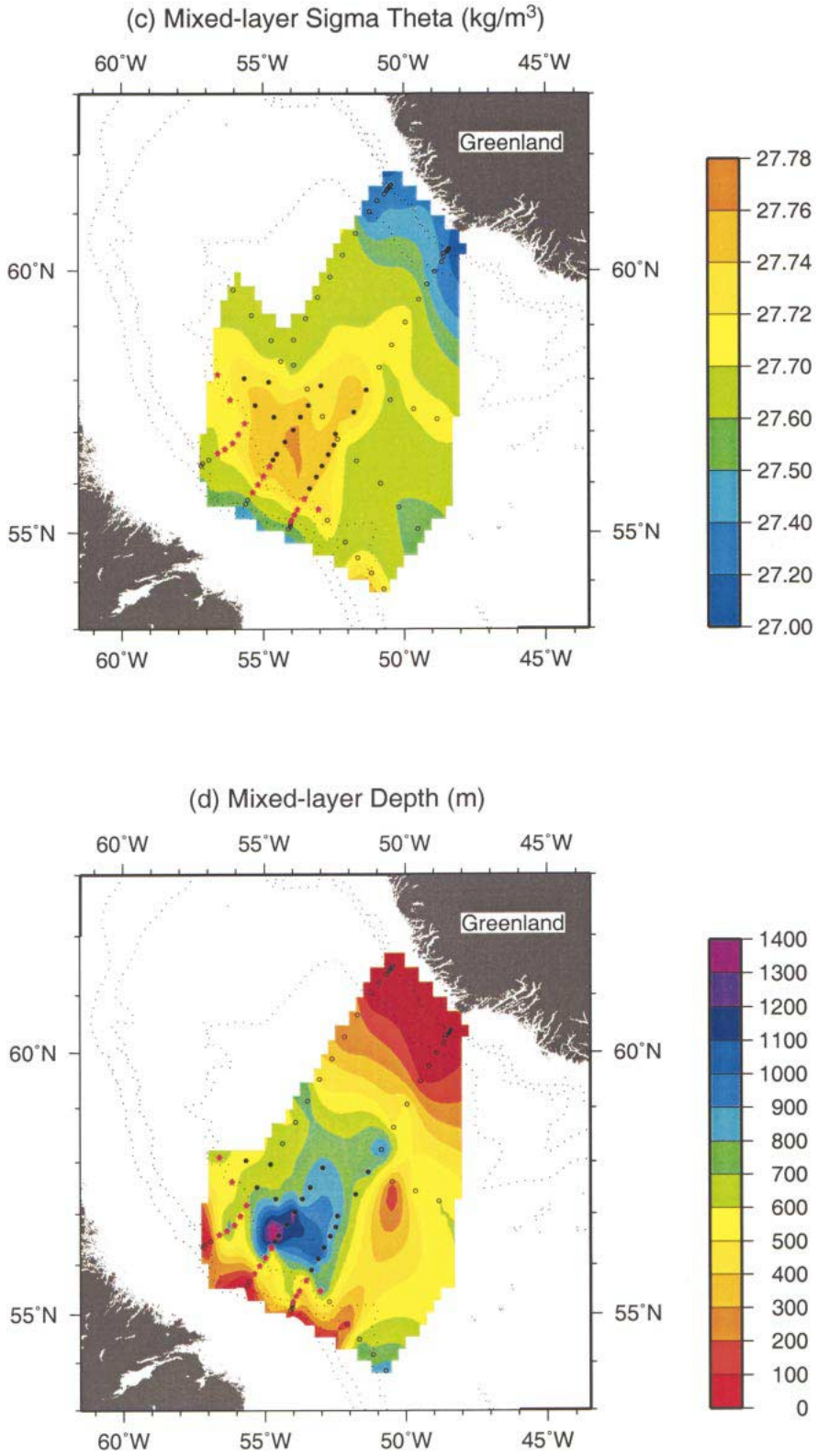


FIG. 12. (*Continued*)

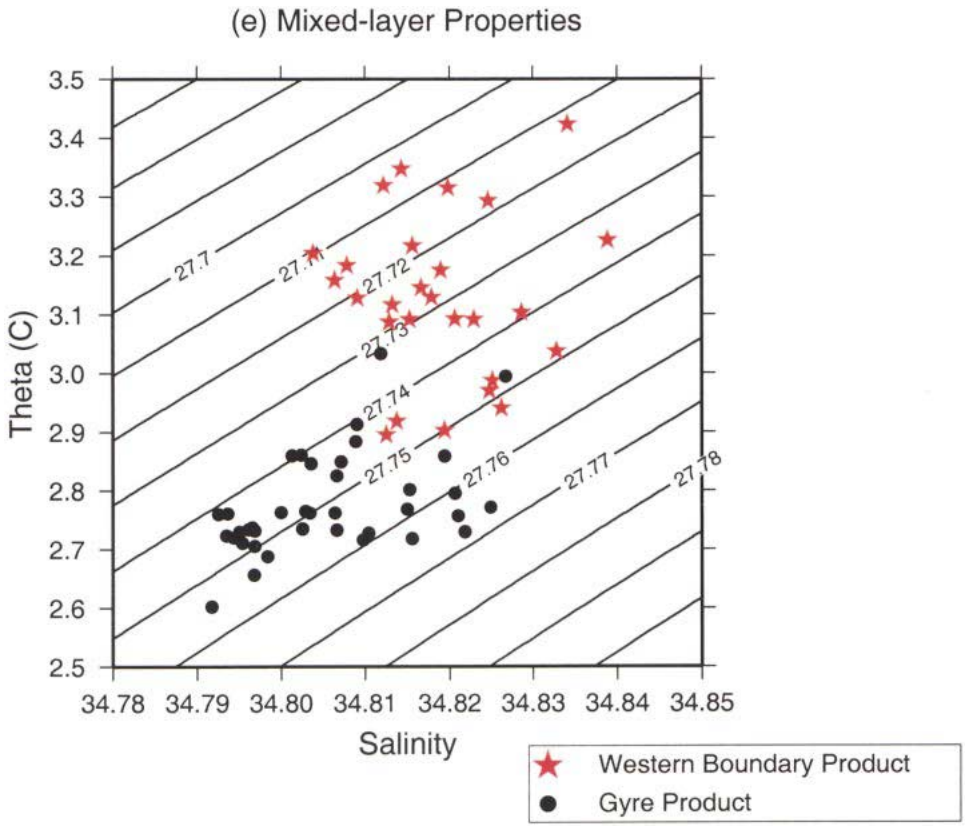


FIG. 12. (*Continued*)

scribed above. However, one feature that is particularly evident in the density field is the anomalous nature of station 92. This station contained buoyant water in the upper layer, which clearly has its origin in the eastern boundary current. A similar feature was also observed in midbasin on the northern hydrographic section of the winter survey (not shown). It is believed that these are in fact remnants of the eastern boundary current rings as discussed above (see also the discussion in section 5b). Based on the seemingly large population of such eddies (Prater 2002; L01b) it is not surprising that we encountered some. Unfortunately, we did not take the time to sample either feature, although some of the RAFOS floats deployed during the Deep Convection Experiment became entrained into eddies in this region, providing some information on their scales (Prater 2002).

### *c. Tracers*

Two common tracers used to identify newly ventilated LSW in the North Atlantic are dissolved oxygen and planetary potential vorticity [PV $\approx (f/\rho)\partial\rho/\partial z$ (Talley and McCartney 1982)]. Our wintertime data allow us to consider the ''boundary conditions'' for these tracers during convective formation. The winter vertical section of oxygen (Fig. 8d) provides important corroborating evidence in identifying the newly convected water. For instance, the boundary current vintage of LSW does not stay unstratified for long (simply because newly formed convective lenses are surrounded by buoyant rim current water). Hence, elevated values of oxygen provide proof that the water was formed in 1997. An example of this is in the Labrador rim current in Fig. 8d: convection has occurred shoreward of station 105, which is not especially obvious in the potential temperature section. This is elaborated on in section 5b.

A striking view of the convective state of the Labrador Sea is provided by the potential vorticity (PV) field (Fig. 8e). The new 1997 water extends to roughly 1000 m. At the time the section was taken, the depth of penetration had not quite reached the body of weakly stratified water remaining from convection in previous years. This deeper LSW was at least two years old because 1996 was a very weak convection year. It is possible that later in the season the thin stratified layer separating the ''old'' and new water was eroded away (we departed the Labrador Sea on 12 March). One can see from Fig. 8e that, if this happened, the depth of convection could easily have reached 2 km as the weakly stratified older water became reventilated. However, evidence of the thin stratified layer, separating the two bodies of water, was present in the spring 1997 occupation of the section. This suggests that convection did

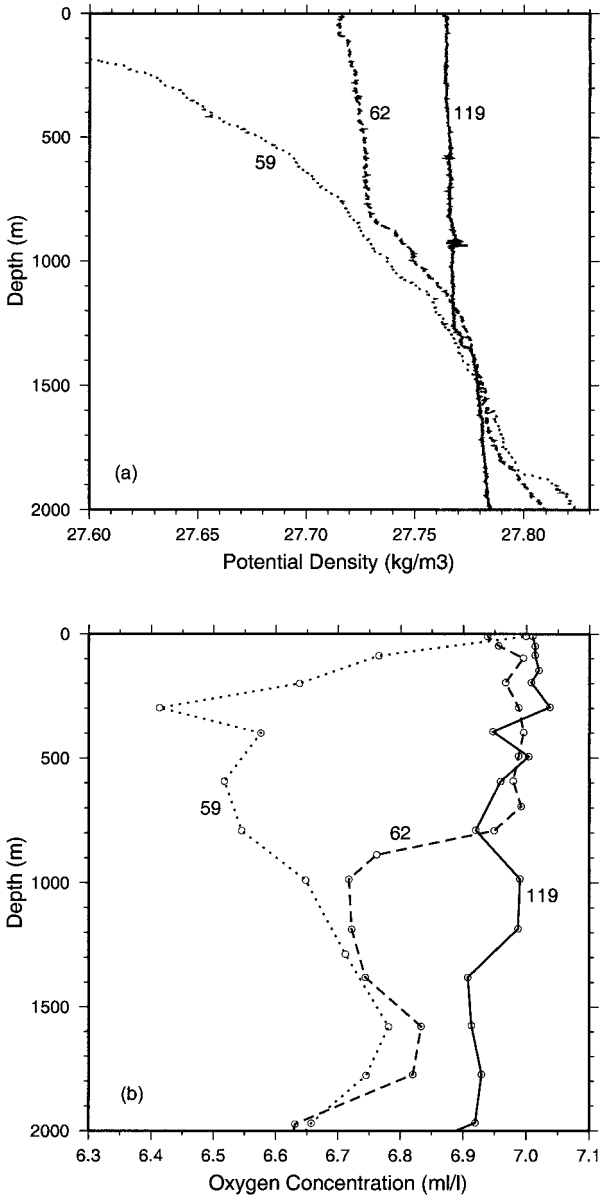


FIG. 13. Vertical profiles of (a) potential density and (b) oxygen concentration from three stations along the central hydrographic line (see Fig. 7). The gyre product (mixed layer depth of 1270 m) is present at station 119 (solid line); the boundary product (mixed layer depth of 825 m) is present at station 62 (dashed line); station 59 was taken in unventilated nearshore water (dotted line).

not penetrate beyond 1500 m during the remainder of the winter. Finally, note the significant presence of the previously formed LSW in the eastern rim current (in both the fall and winter sections); this is another hint of substantial mixing near that boundary.

### *d. Heat storage*

Contrasting the fall and winter potential temperature sections (Fig. 8a), one can visualize the loss of heat from the Labrador Sea as a result of convection. Data from the Deep Convection Experiment allow us to quantify the change in heat storage of the water column and compare it to the strength of the atmospheric forcing. The heat storage $H_s$ is defined as

$$H_s = \rho C_p \theta V, \tag{1}$$

where $\rho$ is the density, $C_p$ is the heat capacity, $\theta$ is the potential temperature, and $V$ is the volume of water. The change in storage along the AR7W line from October to March is shown in Fig. 10. Note the loss of heat associated with the erosion of the upper layer in the center of the basin; as expected, the depth of heat loss extends roughly to 1000 m on the western side. Note that the deeper isolines slant downward toward the west, likely because of the stronger air–sea forcing on that side of the basin.

In the inshore portion of the western rim current there is heat gain near the surface. This is likely an advective effect. In particular, the time period near October represents a maximum in the strength of the baroclinic branch of the Labrador Current, which transports freshwater southward from Baffin and Hudson Bays (Lazier and Wright 1993). The thick cold/fresh layer seen on the western end of the AR7W section in October (Fig. 8b) is likely due to the enhanced presence of this water in the fall. On the eastern side of the AR7W section the heat loss extends to the depth of the Irminger Water despite no local convection there, presumably due to the upstream boundary ventilation scenario described above.

Is the observed heat loss consistent with the forcing? To answer this we limited the area of consideration to the interior of the basin, where advection is weaker. Integrating the heat loss over the portion of the AR7W section delimited in Fig. 10, the net heat loss is $1.04 \times 10^3$ petajoules/kilometer (PJ km$^{-1}$). To estimate the forcing, we integrated the NCEP heat flux over the time period from October to March along the AR7W line. The amount of heat fluxed through the sea surface, calculated as such, was $0.97 \times 10^3$ PJ km$^{-1}$. This good agreement indicates that we can account for the observed change in heat storage in the AR7W section in terms of the regional atmospheric forcing. Formulated as fluxes, the above numbers translate to 202 and 188 W m$^{-2}$, respectively. This represents the average from late October to early March and is reasonable in comparison to the observed average fluxes at Ocean Weather Station Bravo (Pickart et al. 1997b).

## 5. Water mass products

Two different types of Labrador Sea Water have been described in the literature: upper LSW [which has been given other names as well (e.g., Rhein et al. 1995)] and classical LSW. The former is believed to originate in the vicinity of the Labrador shelf break (Pickart et al. 1997b), and is found at relatively shallow depths in the

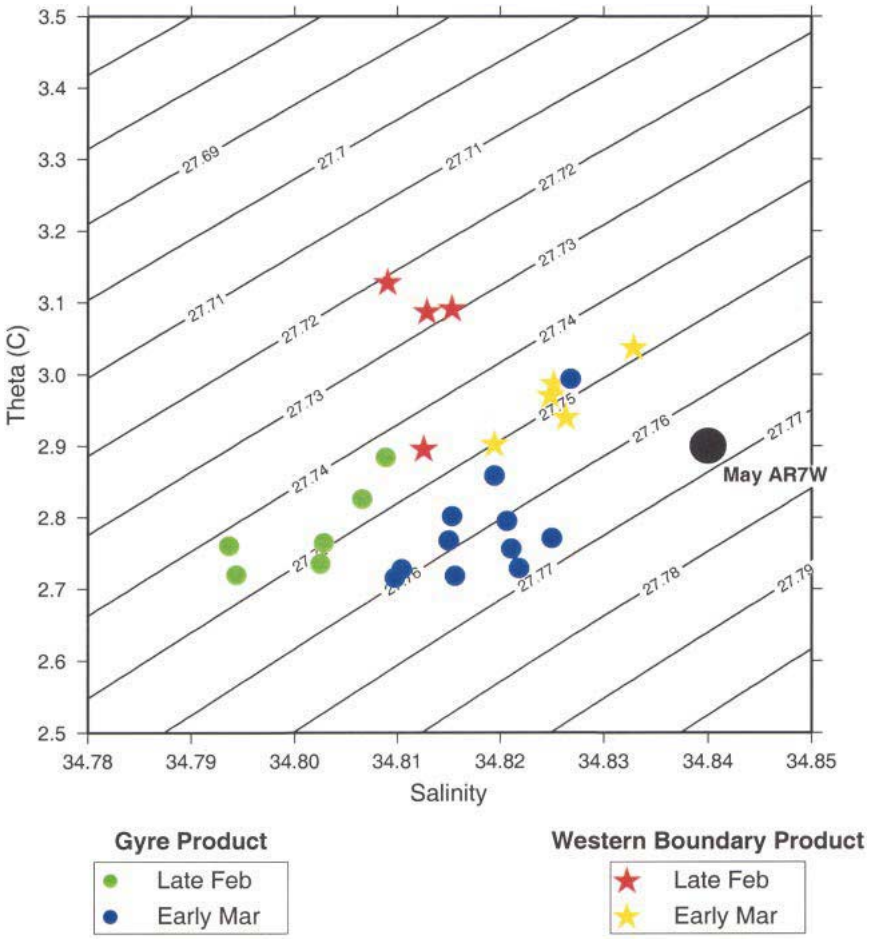


FIG. 14. Time evolution of mixed layer $\theta$–$S$ between the two occupations of Section 2, for the gyre and boundary regions. The final springtime product (see text) is indicated by the large black circle.

North Atlantic. We did not investigate its formation because we were unable to collect data far enough onshore (due to the sea ice, as discussed above). Hence upper LSW is not considered in this paper. The second water mass, classical LSW, is significantly denser and found at greater depths in the North Atlantic (e.g., Talley and McCartney 1982). Its formation, via deep convection, was the focus of our experiment. A central question for the hydrographic cruise was, precisely where does the deep overturning, and hence formation of classical LSW, occur within the Labrador Basin?

The historical notion is that classical LSW is formed seaward of the western continental slope, where the air–sea forcing is strong and the ambient water is most preconditioned (Clarke and Gascard 1983). More recently, Pickart et al. (1997b) reasoned that, in favorable NAO conditions, overturning probably occurs farther south as well, and hence is more readily entrained into the deep western boundary current (DWBC). This latter idea could not be tested in the present experiment because we focused our activities to the northwest where the probability of witnessing convection was greatest. However, one of the major findings of this experiment is that deep convection can occur directly into the DWBC on the western side of the Labrador Sea, as well as in the basin interior. These two geographical regions produce distinct vintages of classical LSW (detailed below). The ''dividing line'' is roughly the 3000-m isobath. Seaward of this we refer to the water mass product as the ''gyre product.'' This is the same water mass that Clarke and Gascard (1983) observed being formed in 1976. Shoreward of this, in the rim current, we call the resultant water mass the ''boundary product.''

### *a. Characterization of mixed layers*

In order to quantify the water mass products, as well as describe the gross characteristics of the observed mixed layers, we systematically identified the depth of the mixed layer in each CTD profile. This was done as a two-step process (Fig. 11). Using the profile of potential density, the approximate extent of the mixed lay-

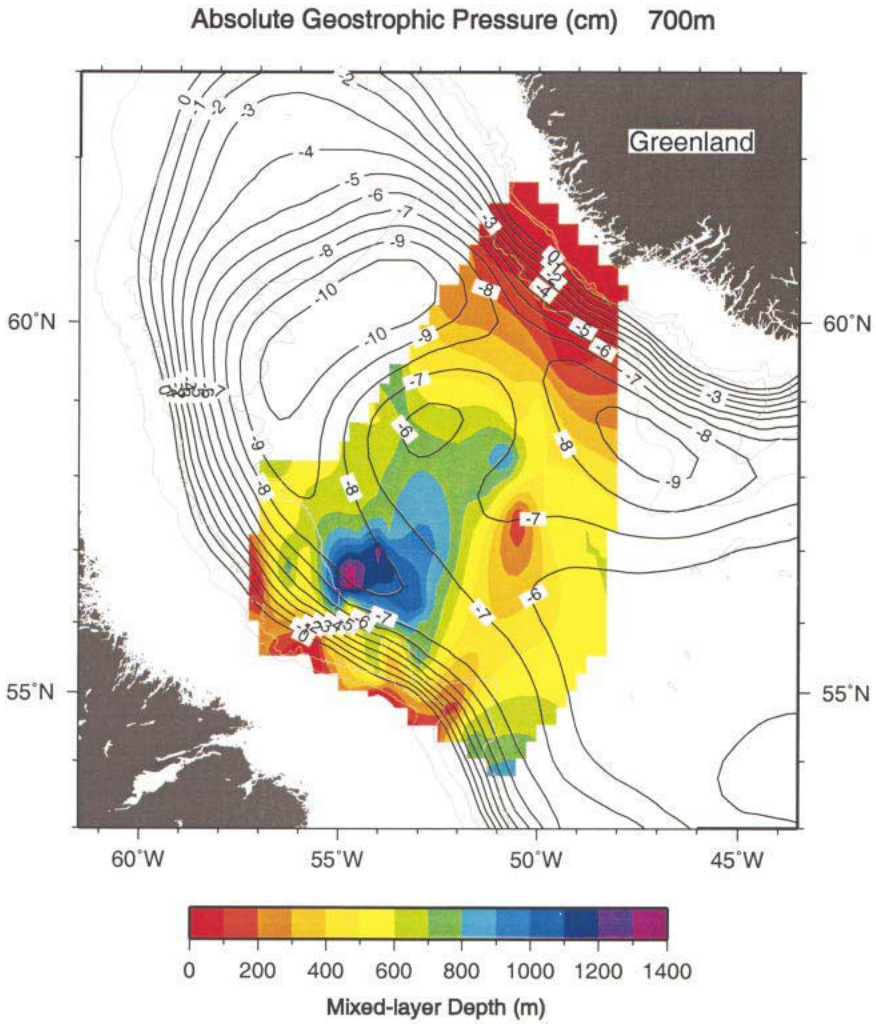


FIG. 15. Mean absolute geostrophic pressure at 700 m as measured by PALACE floats, from Lavender et al. (2000). The mixed layer depth distribution from Fig. 12d is overlaid. Bottom contours are 1000, 2000, and 3000 m.

er was (subjectively) estimated by visual inspection. Then the mean and standard deviation of the density was computed over this depth range, and the two–standard deviation envelope overlayed on the original profile. In the second step we objectively determined the mixed layer depth as the location where the profile permanently crossed outside of the two–standard deviation envelope (Fig. 11). Occasionally (e.g., for particularly noisy profiles) the envelope was used more as a guide, and we subjectively estimated the mixed layer depth. Also, sometimes the above criterion was applied to the potential temperature and/or salinity profiles instead of the density profile. In the majority of the cases, the depth of the mixed layer was easily and unambiguously determined.

One of the interesting features of the hydrographic survey was the occasional occurrence of multiple mixed layers at a single station, which was also observed in the Mediterranean Sea during convective overturning (Schott et al. 1996). In such a case, as the CTD package was lowered from the surface it would pass from one well-mixed region (with a given $\theta$, $S$, and $\sigma_\theta$) through a sharp interface into another well-mixed layer (with distinct properties). Each of the layers was clearly ventilated during winter 1997, so this was not a case of new LSW lying above that formed in a previous winter. It is not clear if such a phenomenon was due to separate layers stacked vertically or to small-scale lateral variability sampled by an instrument that drifted horizontally as it was lowered; or perhaps it was due to slantwise convection. In any case, this condition was observed surprisingly often. There were 31 stations where subsurface mixed layers were measured (at five of these locations two subsurface layers were present). In such cases the mixed layer interface depths were determined in the same fashion as described above.

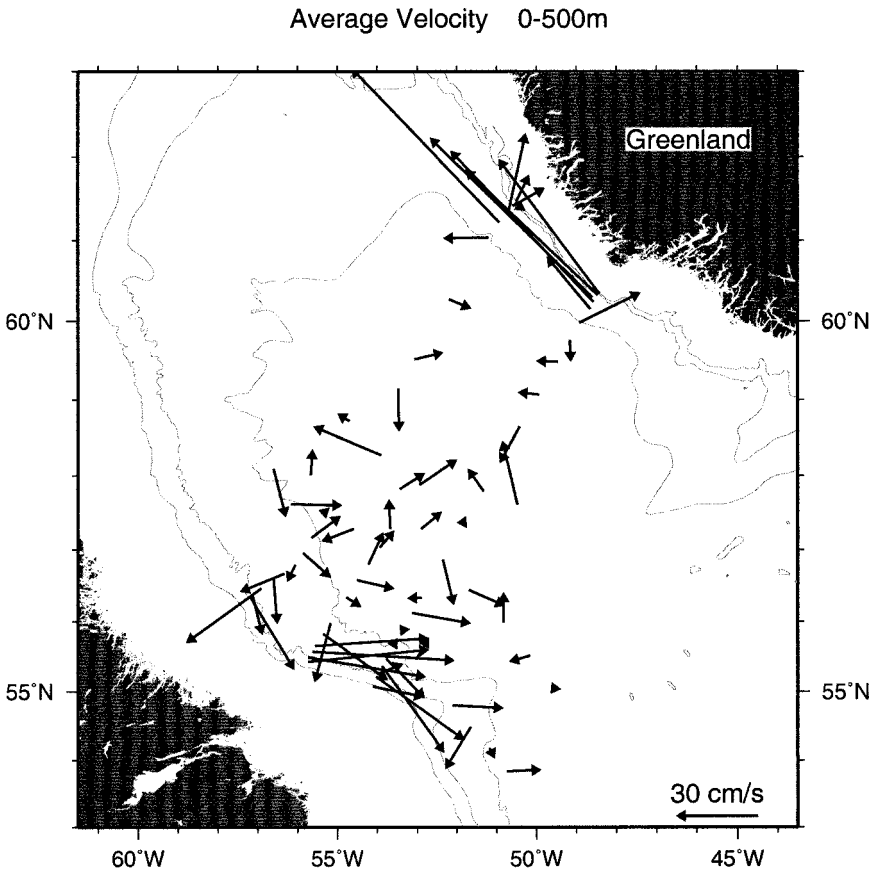


FIG. 16. Flow vectors (averaged over 0–500 m) from the LADCP. Bottom contours are 1000, 2000, and 3000 m.

After the vertical extent of the mixed layer(s) was determined at each station, a simple straight-line fit was applied to the profiles of potential temperature, salinity, and potential density (Fig. 11). Such a fit is meant only to characterize the gross features of the mixed layer. In fact, the observed layers were rich in small-scale [$O$(50–100) m] variability, which is the subject of a separate study. In this paper we take a ''macroscopic'' view and, using the linear fits, consider only the mean properties and stratification of the mixed layer. The reader should note that our use of the term mixed layer does not imply the absence of vertical structure since the majority of the observed mixed layers have nonzero stratification (e.g., Fig. 11). Rather, mixed layer in this context denotes the portion of the water column directly modified by convection, which varies from station to station in stability (see Section 7). In the broad-scale lateral maps presented below, the mixed layer depth corresponds to the depth of the bottom of the deepest layer encountered at the station, while the other properties refer to the mean of the surface-most layer (the difference in properties between the subsurface and surface mixed layers at a given station were small in a large-scale context).

*b. Lateral maps*

The lateral distributions of mixed layer properties (Fig. 12) provide the first broad-scale view of the Labrador Sea during active convection.[2] In the potential temperature field (Fig. 12a), the shelfbreak component of the rim current system is evident by the cold temperatures (due to the Arctic origin of these waters). Seaward of this, the warmer Irminger Water encircles the basin. A puzzle concerning the Irminger signal on the eastern side is that one would expect warmer and saltier values at the southern CTD line (Section 3), not the northern line (Section 1) as observed, simply because the southern line is closer to the upstream source of the water. This can be explained by the eddy generation scenario discussed earlier. The northern CTD line is located in the region of largest eddy activity (Fig. 1). If an eddy breaks off of the rim current and moves

[2] Because of the evolution of the mixed layers over the five-week period of the cruise, there is clearly some temporal aliasing in the lateral maps. This has the most impact on the depth of the mixed layer, and for this reason Section 0 (done first) is not included in Fig. 12d. For the other properties, such aliasing is minor compared to the lateral variation. All maps use the repeat occupation of Section 2.

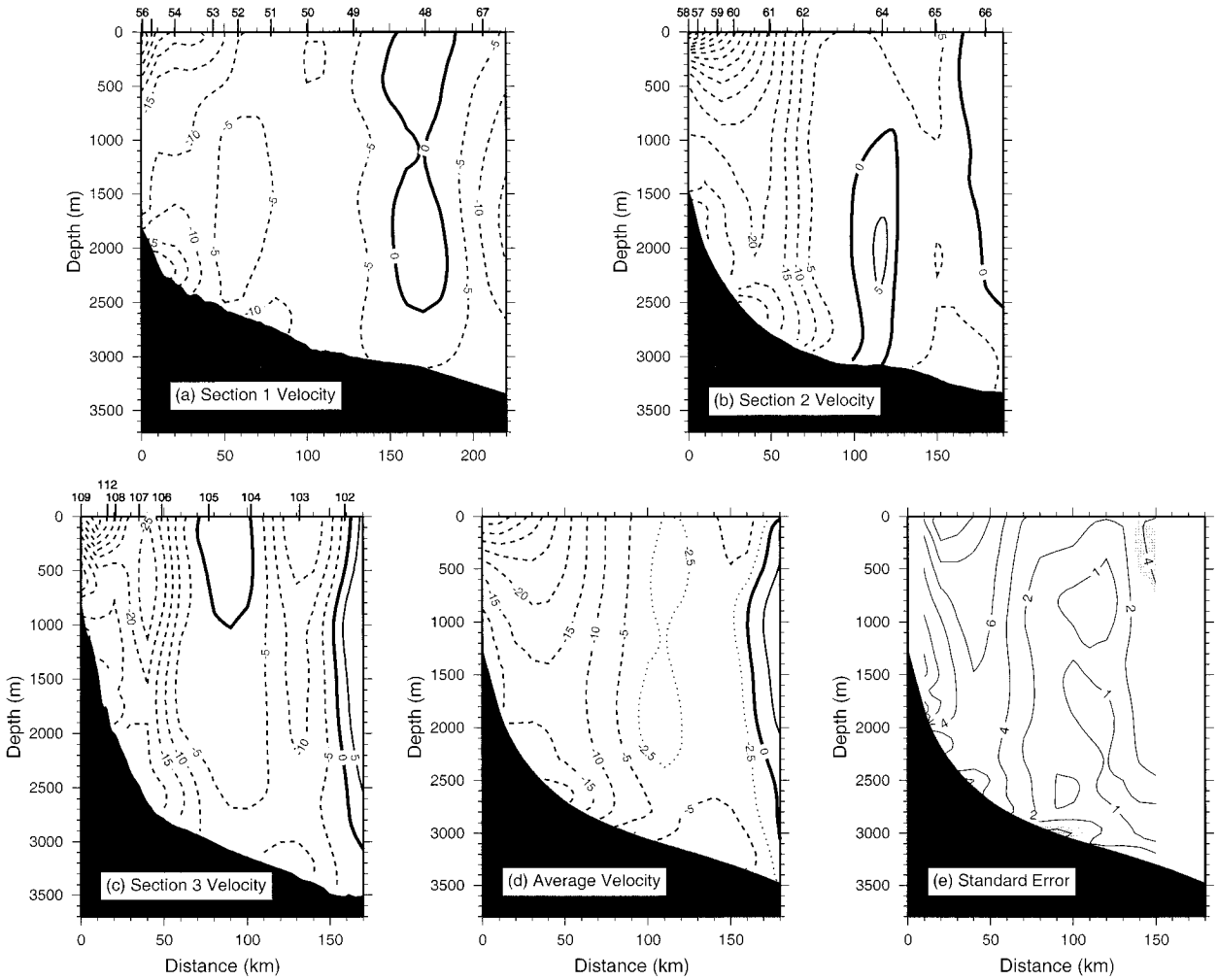


FIG. 17. Vertical sections of alongisobath current (cm $s^{-1}$) from the LADCP (dashed contours are equatorward), for the western end of the three hydrographic lines (see Fig. 7). Transport calculations were done over the length of each section. (a) Section 1; (b) Section 2; (c) Section 3; (d) average of the three sections (see text for explanation of averaging); (e) standard error of the average velocity (gray shading denotes regions where the average is not significantly different from zero).

toward the center of the basin, it brings with it ''pure'' Irminger properties, with a freshwater cap. As it travels seaward it will experience an erosion of properties due to mixing and also be subject to greater air–sea forcing (Fig. 2). Both of these increase the likelihood that convection will occur within the feature, resulting in a warm and salty mixed layer compared to the ambient water. Since the eddy population is likely higher at the northern line, this could explain the unexpected trend in the lateral distribution.

The pool of cold water seaward of the western continental slope is where the densest/coldest/freshest LSW is being formed, that is, the gyre product. This is most clearly seen in the density map (Fig. 12c). Interestingly, the location and lateral extent of the dense pool is very similar to that observed in February of 1978 by Clarke and Gascard (1983), even though that winter was weaker and mixed layers were shallower. In strong winters (i.e., stronger than 1997) deep convection likely occurs over a greater portion of the Labrador Sea [e.g., to the southeast (Pickart et al. 1997b)]. However, the convection is evidently most predisposed to occur in a limited area of the sea. This is discussed further in section 6. As with density, the lateral distribution of mixed layer depth (Fig. 12d) shows an isolated region of large values. However, there is a subtle but important difference: there are some deep mixed layers present over the Labrador continental slope inshore of the densest water. In fact, deep convection also occurred directly within the western rim current, hence forming the boundary product, a lighter/warmer/saltier version of classical LSW. The two products can be seen in vertical plan view in Fig. 8 (stations 93–104 are the gyre product; stations 105–108 are the boundary product). In the lateral maps the two products are denoted by different colored symbols (see caption to Fig. 12).

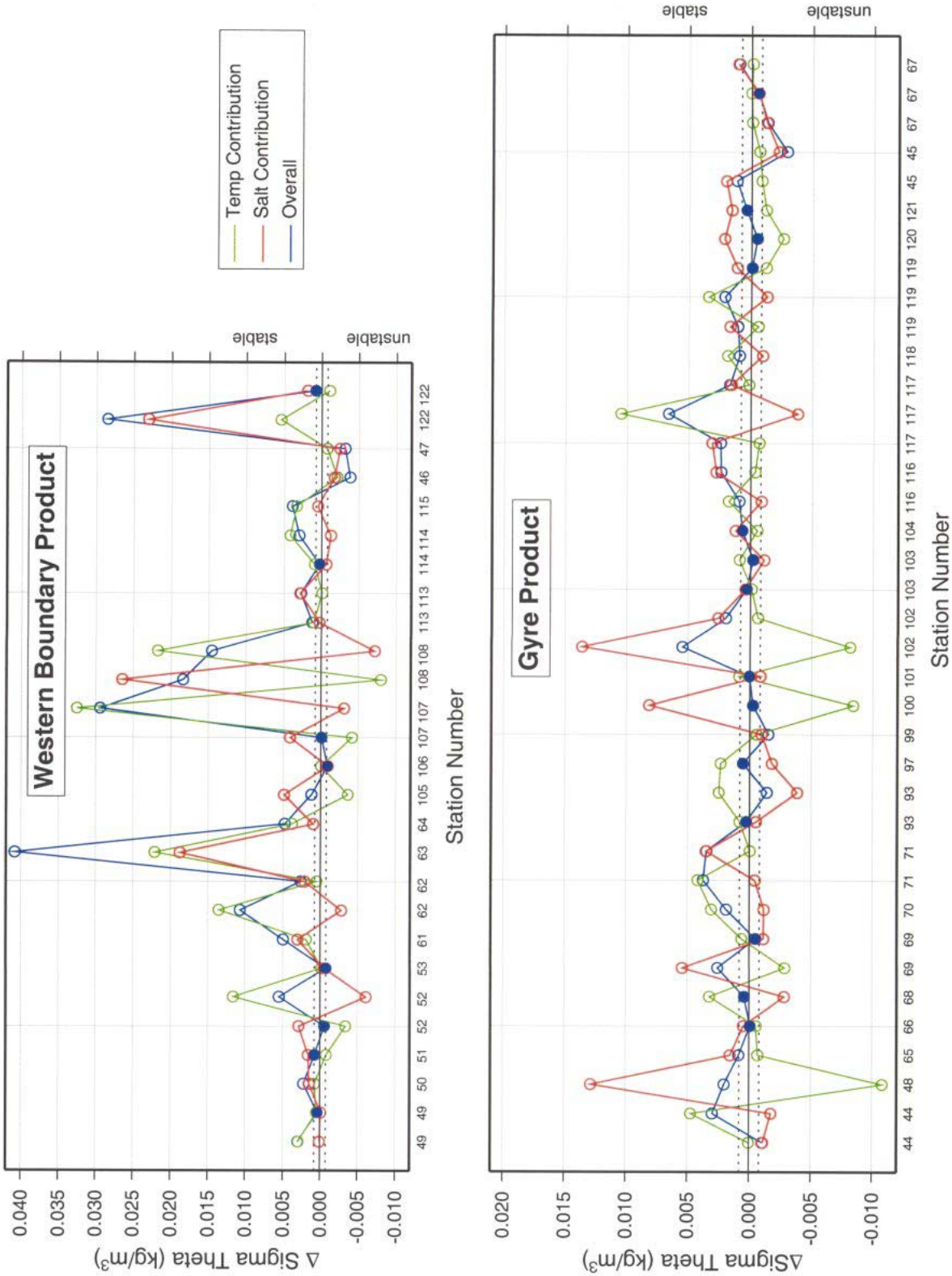


FIG. 18. Change in potential density from the top of the mixed layer to the bottom (blue), including the contribution due to potential temperature (green) and salinity (red). Stations within the dashed lines (filled symbols) are deemed neutrally stable (see text). The station numbers are marked on the abscissa, where repeat numbers correspond to multiple mixed layers at a station (progressing shallow to deep).

### 1) LOCAL BOUNDARY CONVECTION

It is worth examining the possibility that the boundary product is not due to local overturning in the western rim current, but is instead due to convected water from offshore (the gyre product) laterally mixing into unconvected boundary current water. There are several arguments that lead us to discount this notion.

First, although the enhanced stratification near the basin's edge is less conducive for overturning, the air–sea forcing is strongest next to the western boundary. The following simple calculation demonstrates that the observed boundary mixed layer depths are consistent with the atmospheric forcing. The mean speed of the boundary current in the vicinity of the 2500-m isobath is $O(10\ \text{cm s}^{-1})$ (P01b), which means that a water parcel would take roughly 4–5 months to encircle the basin from the eastern end of the AR7W section to the western end. Hence, the western rim current water observed during the winter hydrographic cruise would have been in the eastern basin near the time of the 1996 fall AR7W occupation. Therefore, we chose an eastern boundary profile from the fall section (station 35; Fig. 8) and applied the appropriate NCEP forcing around the edge of the basin—that is, interpolating the NCEP values in the manner of ''following the parcel.'' Using a 1D mixed layer model (Clarke and Gascard 1983; Pickart et al. 1997b), applied in this Lagrangian sense, the depth of overturning reaches 750 m. This is in line with the observed mean mixed layer depth of the boundary product, which is 700 m. (We note that there were several mixed layers in this region that exceeded 900 m, including one as deep as 1130 m.)

A second factor implicating local boundary convection on the western side of the basin pertains to the oxygen saturation of the boundary mixed layers. As reported by Clarke and Coote (1988, their Fig. 2e) the percent oxygen saturation in the newly convected gyre product is on the order of 93%–94%. This is consistent with our observations as well. One would expect that a mixture between this interior water and unventilated boundary water would result in significantly reduced saturation. To test this we considered stations along the central hydrographic line (Fig. 13). Specifically, we computed the percent saturation after mixing—both isopycnally and laterally—station 119 (ventilated gyre product observed late in the cruise) with station 59 (unventilated nearshore boundary water). The resulting saturations of the two mixtures were 91.9% and 91.6%, respectively. This is far less than the 93.9% saturation observed at station 62 (ventilated boundary product). In fact, it is less than the older convected water remaining at depth in the central basin from two winters ago. Hence, the high oxygen saturation of the boundary product argues against a mixture.

A third feature suggesting local overturning is the sharpness of the interface at the bottom of the boundary mixed layers. Consider again station 119 (gyre product) and station 62 (boundary product). Using the (slightly low-passed) $\sigma_\theta$ versus depth profiles, we computed the degree of discontinuity in curvature at the base of each mixed layer and found that it was comparable at the two sites (actually a bit larger for the boundary mixed layer). This is inconsistent with the notion of mixing, whereby a density jump would likely be eroded. Finally, as part of the Deep Convection Experiment, there were moorings situated along the AR7W line, including some within the western boundary current inshore of the 3000-m isobath. Although less conclusive than the hydrography, evidence from mooring records supports the view of local overturning (P. Rhines 1999, personal communication).[3] This should not come as a surprise, since mooring data as far inshore as the 1000-m isobath (from a different winter) indicate a uniform temperature throughout the water column, indicative of local convection [forming upper LSW (Pickart et al. 1997b)].

### 2) LONG-TIME EVOLUTION

The gyre and boundary convective products are clearly distinct in $\theta$ and $S$ (circles vs stars in Fig. 12e). However, convection undoubtedly continued for some time after we left the area; recall that we departed on 12 March, and, according to Lilly et al. (1999), overturning can occur through the end of March. Hence, one might ask, what was (were) the final water mass product(s) formed in the winter of 1997? Our data can shed some light on this question as well. Recall that Section 2 (Fig. 7) was repeated later in the cruise. During the 10 days between occupations the air–sea forcing was particularly strong, and significant evolution of the mixed layer occurred. In Fig. 14 one sees that the gyre product became denser, mainly due to an increase in salinity. By contrast, the boundary product became denser due to cooling as well as salinification. Hence, these two products were converging toward each other in $\theta$–$S$ space.

Further information on the ultimate fate of the water is provided by the springtime repeat of the WOCE AR7W section. As noted earlier it appears that the deeper body of LSW formed earlier in the decade (Fig. 8e) was not reventilated during the winter of 1997. Above this older water, a region of low PV in the springtime section marks the core of the 1997 final product (not shown). The $\theta$ and $S$ of this shallower core are included in Fig. 14. Clearly, further salinification of the mixed layer occurred after our cruise, which is not surprising. Note that the final springtime product is somewhat close to the convergent point of the gyre and boundary products. This suggests that perhaps in the end only a single product was formed (especially after allowing for mixing). Another scenario, however, is that the boundary product, formed directly within the DWBC, was largely

[3] Not all of the moorings, however, show such a signal (U. Send 2000, personal communication).

advected out of the domain by the time of the springtime cruise. A third possibility is that the boundary product restratified to the point where it could no longer be easily detected. These latter two explanations are more likely because most of the low PV core in the springtime section was found seaward of the 3000-m isobath. Hence, the observed final product in Fig. 14 is likely the end state of the gyre water mass, which by spring would be a bit warmer and saltier due to some restratification. [Yashayaev et al. (2000) note that there was broadening of the boundary product *T*–*S* class from fall 1996 to spring 1997, so at least a portion of this product was still present, perhaps due to advection from the north.]

Regardless of the scenario, one would be hard pressed to distinguish between the gyre and boundary convective products any distance away from the Labrador Sea (e.g., at some later time in the eastern Atlantic). For this reason we are not advocating a new water mass name. We are, however, stressing that classical LSW can be formed both within the interior gyre, and within the western boundary current. Using the May $\theta$–$S$ value as the benchmark (Fig. 14), the 1997 value of classical LSW was $\theta = 2.9$°C, $S = 34.84$ psu.[4]

## 6. Circulation

### *a. Mean*

Early descriptions of the general circulation in the Labrador Sea included a weak cyclonic gyre in the center of the basin, with a strong boundary current encircling the sea. Based on modern data, in particular direct measurements, a significantly different pattern has recently emerged. While the notion of a rim current is indeed accurate, the strength of this flow was underestimated in the historical (indirect) measurements. Using moored current meter data, Lazier and Wright (1993) were the first to show that the Labrador Sea rim current has a relatively strong barotropic component over the deep continental slope. Lazier and Wright (1993) argued that this is largely due to the wind-driven Sverdrup return flow of the subpolar gyre, which travels equatorward together with the (bottom intensified) thermohaline overflow water. Farther up the slope, the (surface intensified) baroclinic Labrador Current resides near the shelf break; this is the continuation of the West Greenland Current, with a contribution from the Arctic Ocean via flow through the Canadian archipelago.

The biggest change in our view of the circulation in the Labrador Sea pertains to the interior flow. The dynamic topography of the sea surface (relative to middepth) suggests a basinwide cyclonic flow, corresponding to the doming of the isopycnals towards the center of the sea (e.g., the fall 1996 AR7W section, Fig. 8c). Indeed, this is the basis for the historical circulation diagrams. This pattern was modified, or at least elucidated, by Clarke and Gascard (1983), based on their winter hydrographic data from 1978. These authors introduced the notion of a ''western cyclonic gyre,'' a smaller recirculation that forms during winter in the western half of the basin. This is the baroclinic surface circulation associated with the dense pool that develops during convection (see Fig. 12c). Clarke and Gascard (1983) stressed the importance of this feature in trapping the surface water in the western Labrador Sea, enabling the water to be subject to the air–sea forcing for a longer period, hence resulting in deep overturning.

Using a reference level of 500 db, our 1997 winter data suggest a surface circulation of 1–2 cm $s^{-1}$ in such a western gyre. However, this estimate is purely baroclinic. One of the main observational components of the Deep Convection Experiment consisted of a widespread deployment of Profiling Autonomous Lagrangian Circulation Explorer (PALACE) floats (R. Davis and B. Owens 1997, personal communication; see Lab Sea Group 1998). These data are presented in Lavender et al. (2000) and provide the first direct view of the middepth circulation in the western subpolar Atlantic. The interior pattern can be described as a series of subbasin-scale cyclonic recirculations (four altogether), situated adjacent to the continental slope from the Irminger Basin to the Newfoundland Basin. The mean flow at 700 m in the Labrador Sea, from Lavender et al. (2000), is shown in Fig. 15. As discussed by these authors, the circulation pattern is robust and exhibits little seasonality. Furthermore, the analogous streamline map at 1500 m (Lavender 2000, personal communication) indicates that the flow is largely barotropic. This is verified in P01b for the AR7W section.

Note in Fig. 15 the presence of the cyclonic recirculation southwest of Greenland, and another one of larger extent along the northern and western sides of the basin. Between these, in the center of the Labrador Sea, the flow appears to be anticyclonic (Lavender et al. 2000). This pattern, together with the strength of flow (4–5 cm $s^{-1}$ in the interior at 700 m), suggests that the historical notion of a weak basinwide baroclinic gyre—or western baroclinic gyre—is likely not valid. What drives the subbasin-scale cyclonic recirculations? This is presently an open question, though wind forcing is certainly a factor to consider: recall the strong cyclonic wind stress curl around Greenland that develops every winter (seemingly insensitive to the NAO; Fig. 2).

While a wintertime baroclinic western gyre is evidently not the appropriate conceptual model for the interior Labrador Sea, an analogous feature is present in the absolute circulation in Fig. 15. A distinct trough in absolute dynamic height is situated seaward of the rim current in the western Labrador Sea. While largely barotropic and present year-round—and likely governed by

[4] It should be noted that this is different than the 1997 LSW value quoted by Lazier et al. (2001). Their value ($\theta = 2.85$°C, $S = 34.848$ psu) refers to the deeper PV core, that is, the body of older LSW that was not reventilated in the winter of 1997.

different dynamics—it serves a similar purpose with regard to trapping the water in the region of strong cooling. Hence, one suspects that this should play an important role in dictating the occurrence of convection. This idea is supported by the winter hydrography in that the deepest mixed layers are found within the nearly stagnant center of the cyclonic feature (Fig. 15). Admittedly we are comparing a synoptic distribution with a mean flow pattern, but since the deepest mixed layers in 1978 were also observed here, the agreement is compelling. Also, the PALACE float hydrographic profiles from the winters of 1997 and 1998 showed the deepest mixed layers in this area (Lavender et al. 2000). With the newly formed LSW trapped to some degree in the gyre, this greatly increases the flushing time and provides the means by which the Labrador Sea has a memory of previous winters. It also explains why the 1997 springtime AR7W PV section showed mostly the gyre product that we observed being formed in February. (One also sees how the boundary product is subject to southward advection by the DWBC.)

Why does the deepest overturning not occur farther northward in the cyclonic gyre, where the atmospheric forcing is even greater (Fig. 2)? This is because the ambient water in the northern part of the Labrador Sea is more strongly stratified. As discussed earlier, this stratification is likely due to the buoyant water being fluxed into the northern interior basin from the eastern boundary current via the Irminger eddies. The implication then is profound: that a boundary current instability process—likely related to a local topographic feature—impacts to first order the location and extent of deep convection in the Labrador Sea.

### *b. Winter of 1997*

During our hydrographic survey we had three different means of measuring absolute velocity from the ship: the vessel-mounted ADCP (maximum depth of measurement 500 m), the LADCP (full water column profile at each station), and a hull-mounted acoustic correlation profiler (extending to 1200 m). The latter did not function well under the harsh sea state, so the data return was marginal (an exception to this was the long to-yo, which was done at slow speeds). The LADCP dataset was processed following the procedures in Firing and Gordon (1990) and Fischer and Visbeck (1993), and the resulting measurement accuracy is 2 cm $s^{-1}$. Subsequent to the processing, the data were run through the Oregon State University global altimetric inverse model TPXO.3 (Egbert et al. 1994) to remove the barotropic tidal signal. Finally, each profile was low-passed vertically using a Gaussian filter of width 1000 m (500 m if the water depth was shallower than 1500 m). The purpose of this was to reduce the high wavenumber signal, presumably due to inertial motions and internal waves.

Despite the detiding and smoothing, the LADCP dataset is quite noisy. We believe that this is due to the high eddy-energy levels of the Labrador Sea associated with active convection (e.g., Lilly et al. 1999). This is further supported by the fact that the vessel-mounted ADCP data exhibit very good agreement with the LADCP profiles at the CTD station sites. A lateral snapshot of the flow field during the hydrographic survey, as measured by the LADCP, is shown in Fig. 16. Despite the scatter, the enhanced flow of the rim current system is evident. A vertical view of this current on the Labrador side is provided by the three crossings (Figs. 17a–c, which show the component of velocity parallel to the local isobaths). All three vertical sections show qualitatively the same overall boundary current structure: the enhanced flow of the baroclinic Labrador Current at the onshoremost end of the section, a generally more barotropic signal farther offshore (the wind-driven flow), and some bottom intensification near the 2500-m isobath corresponding to the thermohaline overflow. These components are in line with the earlier moored measurements of Lazier and Wright (1993).

Farther offshore in the vertical sections of Figs. 17a–c the flow is more variable, but predominantly equatorward. We now derive a synoptic transport estimate of the boundary current ''throughput'' versus the adjacent ''recirculation'' revealed by the PALACE data. The total equatorward transports in each of the LADCP sections are 43.5, 49.9, and 43.2 Sv (Sv $\equiv 10^6$ $m^3$ $s^{-1}$) respectively. In light of the scatter in the data, these are surprisingly consistent—and surprisingly large. How much of this transport is the rim-current throughput? Using the 3000-m isobath as the dividing line—which is the approximate division between the boundary and gyre water mass regimes as discussed above—the division is 33.7 $\pm$ 4.2 Sv throughput, and 11.9 $\pm$ 2.1 Sv recirculation (where the uncertainty represents the standard error, assuming 3 degrees of freedom).

Using a mean springtime AR7W geostrophic velocity section, referenced with the mean PALACE velocity at 700 m, P01b objectively computed a throughput rim current transport of 28.5 Sv. According to the diagnostic calculation of Thompson et al. (1986), supported by the direct measurements of Lazier and Wright (1993), the seasonal change in the wind-driven boundary current component between the time period of the winter cruise and the springtime AR7W occupations is approximately 4 Sv. [The change in the baroclinic Labrador Current transport over this same time is negligible by comparison (Lazier and Wright 1993).] Subtracting this from our winter estimate gives 29.7 Sv of throughflow, in good agreement with the 28.5 Sv from P01b. This is consistent as well with Lohmann's (1999) summertime boundary current transport estimates of 27.4 Sv in 1996 and 28.4 Sv in 1997 at the western end of the AR7W line. (These two sections extended 30 km beyond the 3000-m isobath, which would alter our AR7W boundary current estimate by less than a Sverdrup.)

Seaward of the western boundary the velocities mea-

sured by the LADCP are especially noisy and our recirculating transport estimate is less robust. To wit, one notices the regions of northward flow in the vertical sections of Figs. 17a–c (though one would expect poleward flow at the edge of the sections associated with the other side of the cyclonic gyre). Since the velocity profiles have been detided and vertically filtered, it is likely that such scatter is due to mesoscale activity associated with convection. It is therefore advantageous that we have three separate crossings, which when considered together reduces the impact of the variability. To quantify this we constructed an average velocity section from the three realizations, where the averaging was done along isobaths. Specifically, each section was transformed into a bottom-depth coordinate system, averaged, and then the result was transformed back to a distance coordinate system using the average bottom depth profile [see Pickart et al. (1999) for a detailed discussion of the methodology]. The result shows nearly barotropic, weaker equatorward flow offshore of the boundary current (Fig. 17d). While the standard error is generally 30%–40% of the mean (Fig. 17e), the average is significantly different from zero.

The corresponding division in transport calculated from the mean velocity section is 34.2 Sv of throughput and 9.8 Sv of recirculation, comparable to the average of the individual sections. Our wintertime synoptic estimate of the recirculating transport (order 10 Sv) is substantially larger than the springtime mean value computed by P01b (2.5 Sv). In light of the strong flow vectors in the western interior basin and a general cyclonic tendency (Fig. 16), this suggests that there may be seasonal modulation of the gyre (not adequately detected by the floats), with stronger recirculation during winter. The reader should keep in mind, however, the degree of uncertainty in the wintertime estimate when considering this comparison.

## 7. Mixed layer characteristics

We now examine the statistics of the observed mixed layer stratification, which further sharpens the distinction between the boundary product and gyre product—that is, convection within the western rim current versus convection in the interior recirculation. As discussed earlier, the upper layer of the Labrador Sea is generally fresh (Fig. 8b) so that when overturning commences (some time after the cooling has begun) the water column is compensating in $\theta$ and $S$; that is, the ''initial condition'' for convection is cold/fresh water lying atop warm/salty water. Using numerical simulations, Legg and McWilliams (2000) have shown that when overturning occurs in such a fluid, the final convected state is often high in ''spiciness'' while uniform in density—in other words, the resulting vertical gradient in $\theta$ and $S$ are often compensating. This condition has been observed in the Labrador Sea during winter at the Bravo mooring site (Lilly et al. 1999), as well as in the Mediterranean (Schott et al. 1996). What do our hydrographic profiles show? Because of the multiple mixed layers at some of the stations, there are 27 realizations of the boundary product and 38 realizations of the gyre product.

TABLE 1. Mixed layer stratification statistics.

| | Western boundary product (27 stations) | | Gyre product (38 stations) | |
|---|---|---|---|---|
| | Number | Percent | Number | Percent |
| Neutrally stable | 8 | 30 | 14 | 37 |
| Unstable | 2 | 7 | 5 | 13 |
| Strongly stable | 9 | 33 | 2 | 5 |
| Weakly stable | 8 | 30 | 17 | 45 |
| T–$S$ compensating | 11* | 40 | 25** | 65 |

* Six stations were cold/fresh over warm/salty, and five were warm/salty over cold/fresh.

** Thirteen stations were cold/fresh over warm/salty, and 12 were warm/salty over cold/fresh.

We systematically examined the $\theta$, $S$, and $\sigma_\theta$ variation of each mixed layer. These are presented in Fig. 18 and summarized in Table 1, for the gyre and boundary regions. We plot the overall density change from the top of the mixed layer to the bottom, as well as the individual contributions of the density change from potential temperature and salinity. Thus, one can easily identify cases where compensation occurs, that is, where the potential temperature and salinity contributions are oppositely signed (positive means stable stratification, negative means unstable). Changes less than 0.001 in potential density are deemed insignificantly different from zero (this corresponds roughly to 0.01°C and 0.001 psu at these values of $\theta$ and $S$).

The first thing to note is that, in general, the $\theta$, $S$, and $\sigma_\theta$ stratification is stronger in the boundary region (note the difference in scale for the two regions in Fig. 18). This is not surprising because the boundary current is initially more stratified. Second, there are very few instances of unstable density profiles. This perhaps should also be expected, since convective adjustment occurs quite rapidly. However, a significant number of the observed layers are neutrally stable (denoted by the solid symbols in Fig. 18). Among these neutral profiles one can find examples of uniform potential temperature and salinity (e.g., station 49b), weakly compensating temperature and salinity (e.g., station 121), and strongly compensating temperature and salinity (e.g., station 100). Regarding the stable profiles, there are cases where temperature dominates (station 107b), salinity dominates (station 122a), and temperature and salinity contribute equally (station 63).

Both regions have about the same percentage of neutrally stable profiles (Table 1). The gyre region has a larger percentage of weakly stable profiles ($0.001 \leq \Delta\sigma_\theta \leq 0.004$), while the boundary region has a greater percentage of strongly stable profiles. In both regions

roughly half of the mixed layers are compensated in $\theta$ and $S$, while the sense of this compensation is split evenly between warm/salty over cold/fresh and cold/fresh over warm/salty—despite an initial condition of the latter. What are the distinguishing characteristics of the deepest mixed layers? Within the gyre region, the deepest mixed layers are generally the most weakly stratified in density, temperature, and salinity. This is perhaps intuitive: the most intense overturning produces the most weakly stratified product. However, the deepest mixed layers in the boundary region are the most strongly stratified in density. In particular, the temperature stratification generally dominates, since there are salinity gradients of both signs. Hence the deepest products in the two regions represent opposite extrema in terms of stratification—a result that was not anticipated, and should be addressed in future work.

The reader should keep in mind that the above discussion refers to the gross characteristics of the observed mixed layers. In essence this is equivalent to a coarsely resolved view of the water column, for example, similar to what a mooring with discrete instruments would measure or a bottle station. The CTD has a 2-m sampling resolution, and as mentioned above there is substantial small-scale variability within the mixed layers. The type of $\theta/S$ compensation measured by the Bravo mooring and seen in Fig. 18 is of course governed by the macroscopic view. Detailed analysis of the smaller-scale signals will be necessary to fully understand the nature of the overturning and ultimately enable us to parameterize convection in large-scale models. Toward this end, the high wavenumber part of the CTD data is the subject of an ongoing study.

## 8. Summary

A wintertime hydrographic survey in February–March 1997 has provided the first broad-scale view of the Labrador Sea during the period of active convection. Overall, the winter of 1996/97 was moderate and was not typical of either the high or low NAO regime with respect to atmospheric conditions or state of the subpolar gyre. However, during the 5 week period of the cruise the atmospheric forcing was especially strong, characterized by cold air temperatures and strong westerly winds. This resulted in overturning to nearly 1500 m, since the sea was well preconditioned from preceding winters.

A comparison of the WOCE AR7W section occupied in March with that occupied the previous October revealed that familiar cold/fresh/dense classical Labrador Sea Water (LSW) was formed in the western side of the interior basin. The change in heat content in this region implies an average heat loss of $\sim$200 W m$^{-2}$ over the 4-month period, in line with that determined from the calibrated, reanalyzed NCEP model fields of Renfrew et al. (2002). In the eastern Labrador Sea, overturning did not occur because of a strong fresh cap extending from the eastern rim current.

Deep convection was also observed on the western continental slope, directly into the deep western boundary current. This formed a distinct water mass product, somewhat warmer, saltier, and lighter than the familiar interior product. (It would, however, be difficult to distinguish these two types of classical LSW large distances from the Labrador Sea.) An occupation of the AR7W section the following May indicates that the boundary LSW product was either predominantly flushed out of the Labrador Sea or quickly restratified. This is in contrast to the interior LSW product, whose potential vorticity signature was prevalent in the springtime section. This is likely due to the fact that the interior convection occurred within the cyclonic recirculation gyre recently measured by Lavender et al. (2000). Hence, the interior product was trapped to some degree in the western Labrador Sea. Deep overturning did not occur farther north in the recirculating gyre because the ambient water was more stratified, likely due to eddies emanating from the eastern boundary.

The bulk stratification of the mixed layers further elucidates the difference between the boundary and interior classical LSW products. The deepest mixed layers in the interior region tend to be the most weakly stratified (weak in both temperature and salinity stratification), while the deepest mixed layers in the western boundary current are generally the most strongly stratified (due mostly to the temperature stratification). Temperature/salinity compensation was observed in roughly half of the mixed layers in each region, though it should be remembered that the linear trends analyzed here give only a coarsely resolved view. Further analysis of the high wavenumber variability in the mixed layers will be required to permit us to parameterize convection in models.

*Acknowledgments.* We are extremely indebted to Captain A. D. Colburn and the crew of the Research Vessel Knorr for their hard work and dedication in making this field program successful. From the moment we left the dock to the steam back home, the cruise was a constant series of challenges. Each of these challenges was met with professionalism, enthusiasm, and a strong desire to realize the scientific objectives. Whether it was pounding ice off the decks of the ship, navigating through white-out conditions, or maintaining stations near the edge of the pack ice, the crew tackled each test, always maintaining the utmost safety and caution. This was one of the most difficult cruises ever undertaken by a Woods Hole Oceanographic Institution vessel. It was also a striking example of how the makeup of a vessel and the dedication of its crew can impact the success of an experiment. Funding for the cruise was provided by the Office of Naval Research through Contract N00014-97-1-0043. We are indebted to Russ Davis for vocalizing the value of such a cruise, and to

Michael Van Woert for taking the risk and supporting it. We further acknowledge the assistance provided by Dennis Conlon and Tom Curtin in the analysis phase of the experiment. The manuscript was greatly improved as a result of comments from two anonymous reviewers.

## REFERENCES


Belkin, I. M., S. Levitus, J. Antonov, and S.-A. Malmberg, 1998: ''Great Salinity Anomalies'' in the North Atlantic. *Progress in Oceanography,* Vol. 41, Pergamon, 1–68.

Clarke, R. A., and J. C. Gascard, 1983: The formation of Labrador Sea Water. Part I: Large-scale processes. *J. Phys. Oceanogr.,* **13,** 1764–1778.

——, and A. R. Coote, 1988: The formation of Labrador Sea water. Part III: The evolution of oxygen and nutrient concentration. *J. Phys. Oceanogr.,* **18,** 469–480.

Cuny, J., R. B. Rhines, P. P. Niiler, and S. Bacon, 2002: Labrador Sea boundary currents and the fate of the Irminger Sea Water. *J. Phys. Oceanogr.,* **32,** 627–647.

Curry, R. G., and M. S. McCartney, 2001: Ocean gyre circulation changes associated with the North Atlantic Oscillation. *J. Phys. Oceanogr.,* **31,** 3374–3400.

——, ——, and T. M. Joyce, 1998: Oceanic transport of subpolar climate signals to mid-depth subtropical waters. *Nature,* **391,** 575–577.

Dickson, R. R., J. Meincke, S. A. Malmberg, and A. J. Lee, 1988: The ''Great Salinity Anomaly'' in the northern North Atlantic 1968–1982. *Progress in Oceanography,* Vol. 20, Pergamon, 103–151.

——, J. R. N. Lazier, J. Meincke, P. B. Rhines, and J. Swift, 1996: Long-term coordinated changes in the convective activity of the North Atlantic. *Progress in Oceanography,* Vol. 38, Pergamon, 241–295.

Egbert, G. D., A. F. Bennett, and M. G. G. Foreman, 1994: TOPEX/POSEIDON tides estimated using a global inverse model. *J. Geophys. Res.,* **99,** 24 821–24 852.

Firing, E., and L. Gordon, 1990: Deep ocean acoustic doppler current profiling. *Proc. IEEE Fourth Working Conf. on Current Measurements,* Clinton, MD, Current Measurement Technology Committee of the Ocean Engineering Society, 192–201.

Fischer, J., and M. Visbeck, 1993: Deep velocity profiling with self contained ADCPs. *J. Atmos. Oceanic Technol.,* **10,** 764–773.

Hurrell, J. W., 1995: Decadal trends in the North Atlantic Oscillation regional temperatures and precipitation. *Science,* **269,** 676–679.

Lab Sea Group, 1998: The Labrador Sea Deep Convection Experiment. *Bull. Amer. Meteor. Soc.,* **79,** 2033–2058.

Lavender, K. L., R. E. Davis, and W. B. Owens, 2000: Mid-depth recirculation observed in the interior Labrador and Irminger Seas by direct velocity measurements. *Nature,* **407,** 66–69.

Lazier, J. R. N., 1973: The renewal of Labrador Sea water. *Deep-Sea Res.,* **20,** 341–353.

——, 1980: Oceanographic conditions at Ocean Weather Ship BRAVO, 1964–1974. *Atmos.–Ocean.* **3,** 227–238.

——, and D. G. Wright, 1993: Annual velocity variations in the Labrador Current. *J. Phys. Oceanogr.,* **23,** 559–678.

——, R. S. Pickart, and P. B. Rhines, 2001: Deep convection in the Labrador Sea. *Ocean Circulation and Climate,* G. Siedler, J. Church, and J. Gould, Eds., International Geophysics Series, Vol. 77, Academic Press, 387–400.

Legg, S., and J. McWilliams, 2000: Temperature and salinity variability in heterogenous convection. *J. Phys. Oceanogr.,* **30,** 1188–1206.

Lilly, J. M., P. B. Rhines, M. Visbeck, R. Davis, J. R. N. Lazier, F. Schott, and D. Farmer, 1999: Observing deep convection in the Labrador Sea during winter 1994/95. *J. Phys. Oceanogr.,* **29,** 2065–2098.

Lohmann, K., 1999: Gezeitenkorrektur von schiffsgestuetzten Stroemungsmessungen. Diploma thesis, University of Kiel, Kiel, Germany, 86 pp.

McCartney, M. S., 1992: Recirculating components to the deep boundary current of the northern North Atlantic. *Progress in Oceanography,* Vol. 29, Pergamon, 283–383.

Molinari, R. L., R. A. Fine, W. D. Wilson, R. G. Curry, J. Abell, and M. S. McCartney, 1998: The arrival of recently formed Labrador Sea Water in the deep western boundary current at 26.5N. *Geophys. Res. Lett.,* **25,** 2249–2252.

Nielsen, J., 1928: The waters around Greenland. *Greenland: The Discovery of Greenland, Exploration, and the Nature of the Country,* Vol. I, M. Vahl, Ed., C. A. Rietzel, 185–230.

Pickart, R. S., 1997: Adventure in the Labrador Sea: A wintertime cruise to the North Atlantic. *Oceanus,* **40** (1), 18–24.

——, P. Guest, F. Dobson, R. Anderson, K. Bumke, K. Uhlig, U. Karger, and H. Berndt, 1997a: KNORR 147 Leg V cruise summary: Labrador Sea Convection Experiment. WHOI Unpublished Rep., 27 pp. [Available from Woods Hole Oceanographic Institution, Woods Hole, MA 02543.]

——, M. A. Spall, and J. R. N. Lazier, 1997b: Mid-depth ventilation in the western boundary current system of the sub-polar gyre. *Deep-Sea Res.,* **44,** 1025–1054.

——, T. K. McKee, D. J. Torres, and S. A. Harrington, 1999: Mean structure and interannual variability of the slopewater system south of Newfoundland. *J. Phys. Oceanogr.,* **29,** 2541–2558.

Prater, M. D., 2002: Eddies in the Labrador Sea as observed by profiling RAFOS floats and remote sensing. *J. Phys. Oceanogr.,* **32,** 411–427.

Renfrew, I. A., G. W. K. Moore, P. S. Guest, and K. Bumke, 2002: A comparison of surface layer and surface turbulent flux observations over the Labrador Sea with ECMWF analyses and NCEP reanalyses. *J. Phys. Oceanogr.,* **32,** 383–400.

Rhein, M., L. Stramma, and U. Send, 1995: The Atlantic deep western boundary current: Water masses and transports near the equator. *J. Geophys. Res.,* **100,** 2441–2457.

Rhines, P. B., and J. R. N. Lazier, 1995: A 13-year record of convection and climate change in the deep Labrador Sea. *Abstract Report of NOAA Principal Investigator's Meeting,* Miami, FL, NOAA, 50–55.

Rogers, J. C., 1990: Patterns of low-frequency monthly sea level pressure variability (1899–1986) and associated wave cyclone frequencies. *J. Climate,* **3,** 1364–1379.

Ross, C. K., 1992: Moored current meter measurements across Davis Strait. Northwest Atlantic Fisheries Organization Scientific Council Doc. 92/70, 8 pp.

Schott, F., M. Visbeck, and J. Fischer, 1993: Observations of vertical currents and convection in the central Greenland Sea during the winter of 1988–1989. *J. Geophys. Res.,* **98,** 14 401–14 421.

——, ——, U. Send, J. Fischer, L. Stramma, and Y. Desaubies, 1996: Observations of deep convection in the Gulf of Lions, northern Mediterranean, during the winter of 1991/92. *J. Phys. Oceanogr.,* **26,** 505–524.

Smith, E. H., F. M. Soule, and O. Mosby, 1937: The Marion and General Greene expeditions to Davis Strait and Labrador Sea. Scientific results, Part 2, physical oceanography. *Bull. U.S. Coast Guard,* **19,** 1–259.

Steffen, E. L., and E. A. D'Asaro, 2002: Deep convection in the Labrador Sea as observed by Lagrangian floats. *J. Phys. Oceanogr.,* **32,** 475–492.

Straneo, F., and R. Pickart, 2001: Interannual variability in Labrador Sea Water formation and export: How does it correlate to the atmospheric forcing? U.S. CLIVAR Meeting, June 2001, extended abstract volume.

Sy, A., M. Rhein, J. R. N. Lazier, K. P. Koltermann, J. Meincke, A. Putzka, and M. Bersch, 1997: Surprisingly rapid spreading of newly formed intermediate waters across the North Atlantic Ocean. *Nature,* **386,** 675–679.

Talley, L. D., 2000: The shallow, intermediate and deep overturning components of the global heat budget. *Eos, Trans. Amer. Geophys. Union,* **80,** OS52.

——, and M. S. McCartney, 1982: Distribution and circulation of Labrador Sea Water. *J. Phys. Oceanogr.,* **12,** 1189–1205.

Thompson, K. R., J. R. N. Lazier, and B. Taylor, 1986: Wind-forced changes in Labrador Current transport. *J. Geophys. Res.,* **91,** 14 261–14 268.

Wallace, D. W. R., and J. R. N. Lazier, 1988: Anthropogenic Chlorofluorocarbons in newly-formed Labrador Sea Water. *Nature,* **332,** 61–63.

Yashayaev, I. M., R. A. Clarke, and J. R. N. Lazier, 2000: Recent decline of the Labrador Sea Water. International Council for the Exploration of the Sea, CM, 2000/L:18, 10 pp.

Zimmermann, S., T. K. McKee, R. S. Pickart, and W. M. Smethie Jr., 2000: KNORR 147 leg V hydrographic data report: Labrador Sea Deep Convection Experiment. Tech. Rep. WHOI-2000-05, Woods Hole Oceanographic Institution, Woods Hole, MA, 92 pp.